Intense threat switches dorsal raphe serotonin system to a paradoxical operational mode

A Dissertation

Presented to the Faculty of the Graduate School

Of Cornell University

In Partial Fulfillment of the Requirements for the Degree of

Doctor of Philosophy

by

Changwoo Seo

August 2020

Intense threat switches dorsal raphe serotonin system to a paradoxical operational mode

Changwoo Seo, Ph.D.

Cornell University 2020

Survival depends on the selection of behaviors adaptive for the current environment. For example, a mouse should run from a rapidly looming hawk but should freeze if the hawk is coasting across the sky. Although serotonin has been implicated in adaptive behavior, environmental regulation of its functional role remains poorly understood. In mice, we found that stimulation of dorsal raphe serotonin neurons suppressed movement in low- and moderate-threat environments but induced escape behavior in high-threat environments, and that movement-related dorsal raphe serotonin neural dynamics inverted in high-threat environments. Stimulation of dorsal raphe γ-aminobutyric acid (GABA) neurons promoted movement in negative but not positive environments, and movement-related GABA neural dynamics inverted between positive and negative environments. Thus, dorsal raphe circuits switch between distinct operational modes to promote environment-specific adaptive behaviors.

BIOGRAPHICAL SKETCH

Changwoo Seo was born to Sunmi Kim and Jeongwon Seo in Seoul, Korea in 1987. His family moved to the United States of America in 2003. He graduated from Lynbrook High School in 2006. Changwoo then attended Boston University in Boston, Massachusetts, where he majored in Neuroscience. After the second year, he enlisted in the South Korean Army for two years. After the service, he went to Japan where he had his first laboratory experience and learned the patch clamp technique from Dr. Takafumi Inuoe at Waseda University. Then, he briefly worked with Dr. Keiko Tanaka at the Korea Institute of Science and Technology to study the synaptic regulation in the cerebellum. After graduation, he worked with Dr. Kay Tye at the Massachusetts Institute of Technology where he learned optogenetics and animal behavior. In 2013, Changwoo began his doctoral studies in Cornell University's Neurobiology and Behavior program with Dr. Melissa Warden on the role of the serotonin system in motivational behavior.

Acknowledgements

The Ph.D. has been a long and tough journey, but it is not comparable to what my mother and father have gone through to bring me and my sister to this land of opportunity almost twenty years ago. I would not be able to stand here without their love and sacrifices, and I am forever in debt.

This dissertation would have not been possible without my doctoral advisor, Melissa Warden, who was adventurous enough to have me as her first Ph.D. student, and set sail on a new boat together. Your deep insight into science will always be my goal to strive for, and I only hope that someday, I will get there. I thank you for supporting me, believing in me, and being next to me. I could not have a better mentor and a friend like you.

I would like to thank my committee members for mentorship and guidance: Jesse Goldberg for teaching me how to logically question and answer, Joe Fetcho for making me look at the forest of the natural world, and Chris Schaffer for helping me built the fiber photometry set up which was a foundation of all my work.

I would like to thank every amazing Cornell undergraduate whom I worked with including Michelle Jin, Durga Kullakanda, Elias Wang, Christina Boada, Nicholas Krupa, Cynthia Chen, and Alison Sin. You have not only been essential to my dissertation, but also made me a better mentor and a scientist.

I would like to thank every member of the Warden lab: Akash Guru, Ryan Post, Yi-yun Ho, Andrew Recknagel, Dave Bulkin, Yuval Baumel, Wenchao Gu, Brie Sleezer,

Eileen Troconis, and Caleb Vogt for being remarkable colleagues and friends in an out of lab.

I would like to thank all other members of Neurobiology and Behavior department, Teja Bollu, Ruidong Chen, Brendon Ito, Ron Harris-Warrick, and Ron Hoy for scientific help and feedback. Thank you also to Kathie Ely, Saundra Anderson, Lori Maine, Terri Natoli, Sara Eddleman, and Gary Oltz for making me not worry about anything other than science. I am also grateful for my old mentors, Inoue Takafumi, Keiko Tanaka, Hajime Hirase, and Kay Tye, for encouraging me to continue this path.

Lastly, I would like to thank Umji lee for your love and friendship. You make my life happy and meaningful.

Table of contents

LIST OF FIGURES

LIST OF ABBREVIATIONS

5-HT	5-hydroxytryptamine
AAV	Adeno-associated virus
AP	Anterior-posterior axis
ChR2	Channelrhodopsin-2
DRN	Dorsal raphe nucleus
DV	Dorsal-ventral axis
EF1a	Elongation factor 1a
eYFP	Enhanced yellow fluorescent protein
GABA	γ-aminobutyric acid
GCaMP	Genetically encoded calcium indicator
GFP	Green fluorescent protein
LC	Locus Coeruleus
ML	Medial-lateral axis
MRTN	Midbrain Reticular Nucleus
NA	Numerical aperture
NAc	Nucleus Accumbens
OFT	Open field test
PBS	Phosphate-buffered saline
PFA	Paraformaldehyde
PV	Parvalbumin
SERT	Serotonin transporter
SST	Somatostatin

TST	Tail suspension test
VIP	Vasoactive intestinal peptide
VTA	Ventral Tegmental Area

Chapter 1 : Background

“Serotonin is involved in everything, but responsible for nothing”

by B.L. Jacobs

Serotonin (5-HT)

Serotonin (5-hydroxytryptamine, 5-HT) is a major neuromodulatory system that innervates the whole brain and the spinal cord despite its small numbers, only consisting of less than 0.1% of all neurons (Jacobs and Azmitia, 1992). First discovered in blood and the gut as a vasoconstrictor and a gastrointestinal modulator (Souques, 1921; Vialli and Erspamer, 1937), serotonin was later discovered in the brain as a separate system, as the brain serotonin requires a separate biosynthesis and does not cross the blood brain barrier (Côté et al., 2003). Along with other neuromodulatory systems such as dopamine, norepinephrine, and acetylcholine, serotonin is thought to play an important role in a wide range of behaviors, from including sleep, memory, decision-making, social behavior, and emotions.

Notably, the serotonin system has been a major therapeutic target for treating multiple psychiatric disorders, such as depression, anxiety, and panic disorders, due to the accidental discovery that monoamine oxidase inhibitors (MAOIs), which increase serotonin, dopamine, and norepinephrine concentrations in the brain, exert remarkable

mood-enhancing properties (Rowe et al., 1959). In the 1980s, selective serotonin reuptake inhibitors (SSRIs), which increase serotonin levels, were first developed (Hillhouse and Porter, 2015). Compared to MAOIs, SSRIs had similar therapeutic efficacy with less adverse side effects. For these reasons, SSRIs are still first-line medications for treating major depression disorders. However, these drugs do not work on everyone, and more importantly, a mechanistic explanation underlying the treatment-induced remission of psychiatric disorders has yet to be identified. Thus, understanding the endogenous function of the serotonin system will provide new avenues for potential therapeutic interventions.

Serotonin is phylogenetically ancient; found in both the invertebrate and vertebrate nervous systems, it regulates a variety of biological processes including neurodevelopment, synaptic plasticity, neurogenesis, and behavior. Using a crustacean where each neuron is identified in a network, researchers have found that serotonin modulates intrinsic properties of neurons and synaptic efficacy, which enables behavioral flexibility in a fixed neural network (Harris-Warrick and Marder, 1991). Serotonin acts on seven major families of receptors with multiple subtypes; the majority are G-protein coupled receptors, which activate intracellular cascades to produce an excitatory or inhibitory effect on neural activity. These receptors are expressed widely throughout the nervous system, and have unique anatomical, pharmacological, and behavioral profiles that add complexity to understanding the function of serotonin. While serotonin neurons are dispersed around the nervous system in invertebrate organisms, serotonin neurons form distinct clusters in the vertebrate brain. In mammals, nine distinct serotonin neuron

clusters (B1-B9) span from the midbrain through the caudal medulla. The Dorsal raphe nucleus (DRN) and the median raphe nucleus (MRN), located in the rostral part of the brainstem, are mainly connected to the forebrain, while the other nuclei in the caudal brainstem are connected to other brainstems and the spinal cord. In the following sections, I will describe the anatomical and physiological properties of the DRN neurons and review the main theories proposed for serotonergic function.

Dorsal Raphe Nucleus (DRN)

As the name 'raphe' indicates, the DRN is a wing-shaped structure in the brainstem located below the 4th ventricle and the periaqueductal grey. Of the nine serotonin nuclei, the DRN has the highest number of serotonin neurons (1/3 of all serotonin neurons) and provides the largest serotonergic inputs to the whole forebrain. Because of its dense anatomical connections to the forebrain, the DRN has been a major area of study in understanding the function of serotonin in cognition and behavior. The DRN receives brain-wide monosynaptic excitatory, inhibitory and modulatory inputs from the cortex, basal ganglia, amygdala, hypothalamus, and the midbrain (Ogawa et al., 2014; Pollak Dorocic, 2014; Weissbourd, 2014). In return, the DRN also projects widely throughout the forebrain region (Vertes and Linley, 2008). The DRN also contains non-serotonergic neurons including GABAnergic, glutamergic, and dopaminergic neurons, which have common long-range afferent structures (Bang and Commons, 2012; Matthews et al., 2016; McDevitt et al., 2014). Recent studies have shown that the DRN can be divided into anatomically and functionally distinct subregions that have different forebrain

connectivities (Ren et al., 2018). Serotonin neurons can further be divided by the developmental lineage and gene expression profiles (Okaty et al., 2019), however, it is less clear how the heterogeneity in the serotonin system relates to the anatomical connectivity. Overall, the complex input/output architecture of the DRN serotonin system is in line with the modulatory role of serotonin in multiple behaviors.

The recent advancement of molecular and optical tools for neural circuit observation and manipulation in behaving animals have allowed researchers to examine the functional roles of DRN serotonin in specific behaviors. For example, simultaneous recording of the visual cortex (V1) with optogenetic stimulation of DRN serotonin neurons revealed that serotonin suppresses both spontaneous cortical activity and sensory-evoked activity (Azimi et al., 2018). In contrast, activation of DRN 5- serotonin neurons only suppresses spontaneous activity in the olfactory bulb without affecting odor-driven activity (Lottem et al., 2016). If DRN serotonin modulates neural coding properties, how does it affect behavior? The type of behavior that is influenced by serotonin may depend on the downstream site of DRN serotonin release. The amygdala or the bed nucleus of the stria terminalis (BNST) encode fear- and anxiety-related information, and inactivation of these structures impairs the acquisition and expression of fear-related behaviors (Anglada-Figueroa and Quirk, 2005; Kim et al., 2013). Optogenetic activation of DRN serotonin projections to these structures changes firing rates of the downstream neurons and modulates fear-related behavioral expressions. DRN serotonin is also involved in establishing social rewards, since genetic disruption of the DRN serotonin input to the nucleus accumbens (NAc) results in impaired social interactions (Dölen et al., 2013). With

the advances in manipulating genetically identified, pathway-specific DRN serotonin neurons, we now have a better understanding of how DRN serotonin is involved in modulating specific aspects of firing properties of the downstream brain regions and behavior. However, how do we understand the function of the system that has a small number of neurons, but has the diversity of receptors expressed widely throughout the brain, and is involved in a broad spectrum of behaviors?

Theories of serotonin

To better understand the serotonin system, multiple theories have been proposed in an attempt to unify various findings. I will review three major theories: 1) behavioral inhibition; 2) aversive processing; and 3) reward processing theory.

In the 1980s, it was proposed that serotonin promotes behavioral inhibition based on findings that decreased serotonin leads to persistent action attempts for reward even when there is no more subsequent reward present (Soubrié, 1986). Subsequent studies looked at the behavioral impacts on impulsivity and compulsivity, where animals were required to actively withhold actions to complete a task. Electorophysiological recording of putative DRN serotonin neurons showed increased firing rates during the delay period, and the stimulation of DRN serotonin neurons prolonged the waiting period (Miyazaki et al., 2011, 2012, 2014). The authors suggest that simple behavioral inhibition may be not be an adequate description and serotonin is involved in higher cognitive function.

Selective activation of a genetically-targeted serotonin population results in similar behavioral inhibition phenotypes across different organisms including *C. elegans*, drosophila, zebra fish, and mice (Correia et al., 2017; Flavell et al., 2013; Howard et al., 2019; Kawashima et al., 2016). These findings suggest that there may be an evolutionarily preserved mechanism of behavioral inhibition phenotype due to serotonin activation, however, serotonin's computational role in behavior remains unknown. Interestingly, serotonin-releasing neurons in *C. elegans* play a major role in sensing food availability, which is an important factor in switching between exploit and exploratory behavior (Flavell et al., 2013). It is possible that serotoninergic influence on behavioral inhibition has evolved to meet certain sensorimotor needs, and later became adopted in higher cognitive functions.

Deakin and Graeff propose that serotonin is involved in the aversive learning process by inhibiting undesired behavior under negative contexts (Deakin and Graeff, 1991) with evidence that depletion of serotonin in pigeons impairs the suppression of pecking behavior with a contingent footshock (Graeff and Schoenfeld, 1970). While similar to Soubrié's behavioral inhibition theory, the theory was later extended to suggest that the computational role of serotonin is to carry negative prediction error signals and drive aversive learning in comparison with the dopamine system, which shows positive prediction error-like neural activity (Boureau and Dayan, 2011; Daw et al., 2002). However, recent studies recording mouse DRN serotonin neurons under both reward and aversive learning tasks demonstrated that serotonin neuron activity represents a variety of learning-related signals beyond only negative prediction error signals. For example,

after successfully demonstrating that VTA dopaminergic neurons encode reward prediction error signals, Cohen et al. used the same optically-tagged electrophysiology recording techniques and behavioral tasks to examine whether DRN serotonin neurons encode negative prediction error signals. Animals were presented with three distinct odors paired with either water, air puff, or no outcomes. Then, each odor-outcome pair was presented multiple times for the duration of five minutes until the next pair was presented for the same duration (Cohen et al., 2012, 2015). Instead of encoding negative prediction error-like signals, optically identified DRN serotonin neurons exhibited two types of responses: a variety of phasic responses to odor cues and outcomes, and tonic, minute-lasting, firing rate changes that followed the valence of the trial blocks (ex, increased firing rate for the reward block compared to the punishment block). Another study monitoring the average activity of DRN serotonin populations using calcium imaging in a similar odor-paired reward/punishment outcome task revealed that the DRN serotonin system showed a complex and incomplete form of prediction error-like signals (Matias et al. 2017). In line with these findings, researchers have established that activation of DRN serotonin neurons can enhance both fear and reward learning (Liu et al., 2014; Marcinkiewcz, 2016; Sengupta and Holmes, 2019). Unlike the dopaminergic reward prediction error signals which can be quantitatively conceptualized, we cannot yet fully describe the activity patterns of the DRN serotonin system, and the recent findings raise concerns about interpreting the aversive processing theory.

Lastly, some findings suggest that DRN serotonin neurons encode reward-related signals. Electrophysiological recordings in awake primates during a reward-seeking

behavior demonstrated that DRN neuron activity was characterized by expected and received reward values, similar to the finding by Cohen et al. 2015 (Bromberg-Martin et al., 2010; Nakamura et al., 2008). The authors suggest that these features may play an important role in reinforcement learning by providing necessary information to the dopamine neurons for calculating prediction error signals (Nakamura, 2013). Another group performeda recordings from identified DRN serotonin neurons using optically-tagged electrophysiology and calcium imaging, and they have also reported similar findings, albeit with some differences in the exact timing of serotonin activity during the reward task. This study has expanded the role of DRN serotonin neurons, showing how they carry reward value signals that can be generalized to different behaviors such as feeding, social interaction, and mating (Li et al., 2016). The same group also demonstrated that activation of DRN serotonin neuron results in positively reinforced behavior (Liu et al., 2014). Overall, the authors propose that DRN serotonin neurons encode 'beneficial signals' at a given context to maximize behavior that is most appropriate, and their research attempts to reconcile previous findings regarding behavioral inhibition and aversive processing theory (Luo et al., 2016). They also argue that the efficacy of the 5-HT system driven antidepressants to increase mood and motivation has an underlying 'beneficial' mechanism.

While these theories capture various findings related to the serotonin system, the modulatory role of serotonin also extends to sleep, sensorimotor modulation, thermoregulation, and feeding, etc. Current theories are either too narrow and explain only a subset of findings, or they are too wide and cover many factors without being able

to explain details. Then, how do we come up with a general principle of serotonin that can describe a global function? One hope is that with more controlled and comparable descriptions of DRN serotonin neuron activity in multiple contexts, we will be able to find the right spot in the theoretical spectrum. In my dissertation work, I characterize the endogenous activity of the DRN system to better understand how the signals arise, and I manipulate these neurons to identify causal relationships with behavior.

Chapter 2 : Dorsal raphe serotonin neuron activity promotes opposite behaviors in high-threat and low-threat environments

Animals need to move in order to survive. Sometimes animals move to pursue necessities such as food or water or a mate, and sometimes they move to flee from a predator or to avoid a risky situation. The decision to move or to refrain from movement, and when and where to move, depends on the structure of the environment and the internal state of the animal (Berridge, 2004; Deakin and Graeff, 1991; Fadok et al., 2017; Fanselow and Lester, 1988; De Franceschi et al., 2016). An immediate threat may provoke a fast, reflexive escape movement, while a more distant or uncertain threat may induce either the inhibition of movement or, if a route to safety is available, a delayed, strategic avoidance response. Similarly, a hungry animal may move to seek out an available food source even in the face of potential risk, while a sated animal may not find this goal worth the cost. Regulation of movement depends on the interaction between environmental context and internal state, and different environment-state combinations may shift the balance of activity between different neural circuits in order to facilitate appropriate behavior (Miller et al., 2017).

Neuromodulatory systems are essential for the high-level, coordinated regulation of the neural circuits that control movement. These systems receive input from regions of the brain that represent environmental structure and internal state, and project widely to cortical, striatal, brainstem, and spinal regions involved in the control of movement. While

dopamine is thought to play a central role in promoting behavioral activation(Salamone and Correa, 2012) and vigor(Niv et al., 2007), as illustrated by the movement-facilitating action of dopamine-enhancing psychostimulants and the reduction in movement accompanying the degeneration of dopamine neurons in Parkinson's disease, forebrain serotonin (5-hydroxytryptamine; 5-HT) has been more robustly associated with behavioral inhibition. Elevated 5-HT has been shown to promote inactive behaviors such as the ability to wait patiently for rewards or to withhold previously punished responses, while reduced 5-HT has been associated with increased impulsivity, the inability to inhibit premature responses in reward tasks, and faster acquisition of conditioned avoidance behavior.

Paradoxically, given the association of elevated 5-HT with behavioral inhibition, acute administration of selective serotonin reuptake inhibitor antidepressants immediately before behavioral testing promotes escape behavior in the tail suspension test(Jin et al., 2017), a widely employed behavioral test for depression-like states in rodents. This drug-induced increase in mobility, not present in the open field test, suggests a context-dependent role for 5-HT in regulating movement. An effect which may have relevance for context-dependent movement regulation is that changes in environmental structure have been shown to affect the baseline activity of 5-HT neurons. The recent history of rewards or punishments in classical conditioning paradigms strongly modulates baseline 5-HT firing rates, suggesting that this activity may reflect an animal's assessment of local state value (Cohen et al., 2015a; Hayashi et al., 2015). Further, inescapable stress leads to activation and long-lasting sensitization of 5-HT neurons and a robust increase in 5-HT

release, but identical escapable stress does not,(Grahn et al., 1999; Maier and Watkins, 2005; Maswood et al., 1998) suggesting that 5-HT activity can also reflect an animal's assessment of the degree to which it controls the environment. Environmentally-driven changes in tonic 5-HT firing may recalibrate the dynamic range of adaptive behaviors modulated by downstream neural circuits.

We used fiber photometry(Gunaydin et al., 2014) to monitor the real-time neural dynamics of genetically defined DRN 5-HT neurons in freely behaving mice (fig. S1A). We injected Cre-dependent AAV5-CAG-FLEX-GCaMP6s (Chen et al., 2013) into the DRN of SERT-Cre mice to express a genetically-encoded calcium indicator, GCaMP6s(Chen et al., 2013), in DRN 5-HT neurons.(Zhuang et al., 2005). We then implanted an optical fibre over the DRN to deliver excitation light and monitor calcium-dependent fluorescence (Fig. 1A and fig. S1B). As transient optogenetic stimulation of DRN 5-HT neurons has been shown to decrease speed in the open field (Correia et al., 2017), we recorded neural activity while mice were freely moving around in the open field test (OFT, Fig. 1B). Examination of the bulk fluorescence activity of DRN 5-HT neurons at movement onset in the OFT) was associated with a robust reduction in DRN 5-HT fluorescence), an effect that we did not detect in control GFP-expressing mice (Fig. 1, C to E; GFP control data, Fig. 1E and fig. S1, C to E).

To gain more insight into the role of the environment in shaping the movement-related dynamics of DRN 5-HT neurons, we recorded neural activity while mice performed active reward-seeking and punishment-avoidance behaviours, chosen because DRN 5-

HT neurons exhibit tonic firing rate changes between reward and punishment blocks in Pavlovian tasks(Cohen et al., 2015a; Hayashi et al., 2015). Mice were first trained on a cued reward approach task (Fig. 1F and fig. S2, A and B), in which they heard an auditory cue and crossed the chamber midline before cue offset in order to receive a reward. We found that DRN 5-HT neural activity decreased on movement onset in this environment, consistent with the reduction observed upon movement onset in the open field (Fig. 1, G to I). At movement offset, we observed recovery of decreased DRN 5-HT neural activity (Fig. S3, A and B).

We then trained mice on a cued avoidance task (Fig. 1J), in which they heard an auditory cue and crossed the chamber midline before cue offset to avoid a shock. DRN 5-HT neural activity also decreased during cued movement to avoid the shock (Fig. 1, J to M, and fig. S2, C and D; movement offset, fig. S3, C and D), a finding that may reflect behavioural control over shock exposure(Amat et al., 1998; Maswood et al., 1998). Thus, we have demonstrated a general reduction in DRN 5-HT neural activity during movement in positive or mildly negative environments.

Figure 1

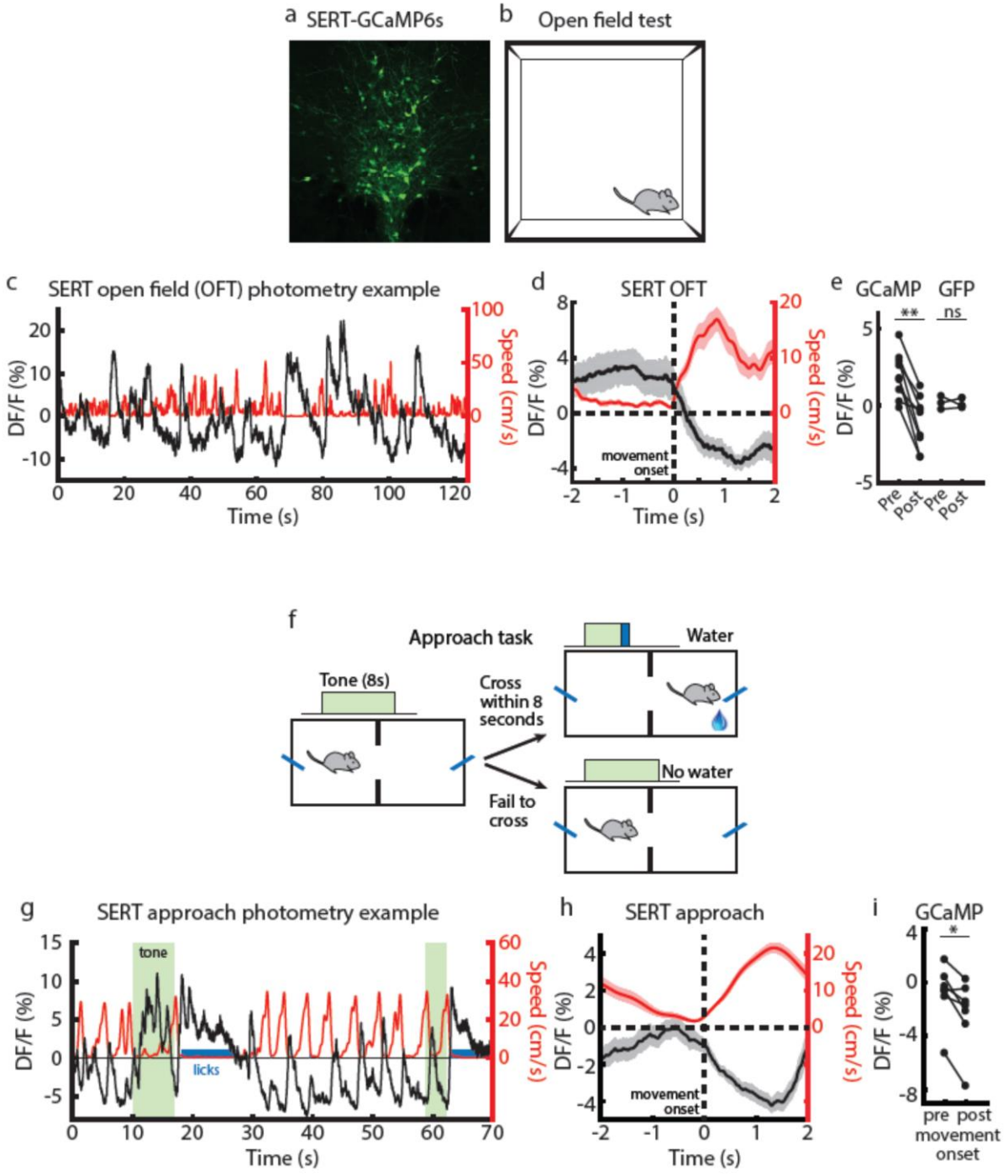
a SERT-GCaMP6s
b Open field test
c SERT open field (OFT) photometry example
DF/F (%)
Speed (cm/s)
Time (s)
d SERT OFT
movement onset
e GCaMP GFP
**
ns
Pre Post Pre Post
f Approach task
Tone (8s)
Cross within 8 seconds
Water
No water
Fail to cross
g SERT approach photometry example
tone
licks
h SERT approach
movement onset
i GCaMP
*
pre post
movement onset

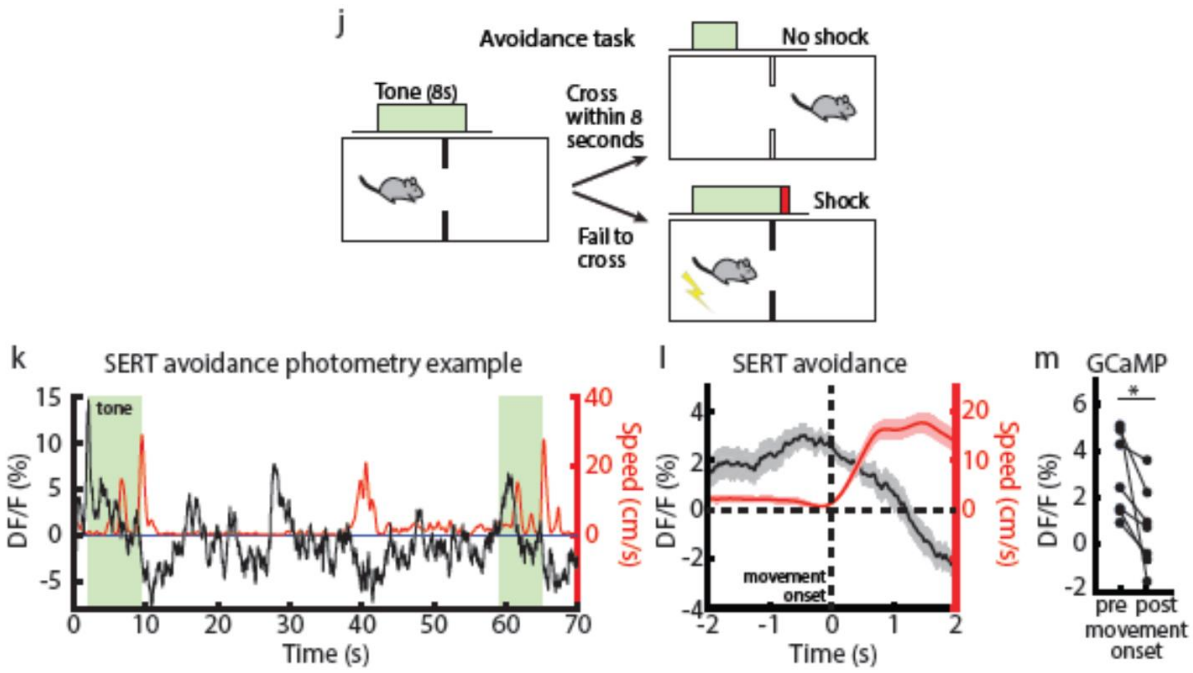

Fig. 1.

DRN 5-HT neural activity decreases upon movement in low- or moderate-threat environments.

(**A**) GCaMP6s expression in DRN 5-HT neurons in a SERT-Cre mouse. (**B**) OFT schematic. (**C**) Example OFT photometry from a SERT::GCaMP6s mouse. GCaMP ΔF/F in black, speed in red. (**D**) Mean ΔF/F aligned to OFT movement onset. (**E**) Mean ΔF/F before and after OFT movement onset in GCaMP (n=9) and GFP (n=3) mice. (**F**) Approach task schematic. (**G**) Example approach photometry from the same mouse. (**H**) Mean ΔF/F aligned to approach movement onset. (**I**) Mean ΔF/F before and after approach movement onset in GCaMP (n=7) mice. (**J**) Avoidance task schematic. (**K**) Example avoidance photometry data from the same mouse. (**L**) Mean ΔF/F aligned to avoidance movement onset. (**M**) Mean ΔF/F before and after avoidance movement onset

in GCaMP (n=7) mice. *P < 0.05, **P < 0.01, Wilcoxon signed-rank test. Error bars indicate s.e.m.

Next, we examined DRN 5-HT neural activity during the TST (Fig. 2A), a high-threat environment often used for probing active and passive stress-coping behaviours in mice(Commons et al., 2017). Mice were suspended by their tail for a period of several minutes, and transitions between escape-related struggling behaviour and immobility(Warden et al., 2012) were monitored with an accelerometer (Commons et al., 2017). We discovered that TST struggles correlated with a robust increase in DRN 5-HT fluorescence (Fig. 2B), unlike movement in the open field, cued approach, or cued avoidance tasks (Fig. 1). Transitions from immobile to mobile states were associated with increased neural activity, an effect not detected in control GFP mice (Fig. 2, B to D; GFP data, Fig. 2D and fig. S1, F to H; movement offset fig. S3, E and F)

Unlike the other behavioural testing environments, which are either rewarding or controllable, the unconditioned aversive stimulus is unavoidable in the TST. Being hung up by the tail is extremely stressful(Bruchas et al., 2007; Commons et al., 2017; Deakin and Graeff, 1991; Lemos et al., 2012), and the active coping (struggling) exhibited during the TST is similar to the active defensive behavior (flight) observed in models of proximal threat(Deakin and Graeff, 1991; Fadok et al., 2017) This environmental feature may underlie the emergence of altered DRN 5-HT signalling during movement in the TST. To test this hypothesis, we examined DRN 5-HT neural dynamics during failed trials in the cued avoidance task, in which the mouse did not cross the chamber quickly enough to avoid shock onset. In these trials mice ran to escape the ongoing shock, which terminated when they crossed the chamber midline. Consistent with this interpretation, we observed a robust increase in DRN 5-HT fluorescence during shock-induced escape movements

(Fig. 2, E and F) , in which mice were similarly in direct contact with the stressor. Thus, in most environmental contexts movement is correlated with a dip in DRN 5-HT neural activity, but in high-stress escape situations movement is instead correlated with increased activity.

We demonstrated that the population DRN 5-HT neural activity switches during movement onset in high threat environments, but it remains unknown whether individual DRN 5-HT neurons switch their response properties. Alternatively, different populations of DRN 5-HT neurons connected to other brain areas may selectively respond depending on the condition. To address this, we performed in vivo microendoscopic imaging of single DRN 5-HT neurons expressing GCaMP6s in SERT-Cre mice during sequential engagement in the open field test (OFT) and tail suspension test (TST) (fig. S4, A to C). Within the group of neurons significantly selective for movement in both tests (54%, 13/24), neurons with movement dynamics that inverted between tests comprised 62% (8/13) of the population (fig. S5B, examples in fig. S4, D to H and fig. S5, A and C). Many neurons showed elevated activity during movement in the TST, and these neurons typically responded during all TST movement events (fig. S5A). Interestingly, within this group different subsets of neurons showed elevated activity during different pauses in movement in the OFT, suggesting enhanced response complexity in this environment (fig. S5A). Thus, DRN 5-HT neural activity decreases on movement initiation in low- or moderate-threat environments, but high threat, escape-provoking environments invert this response.

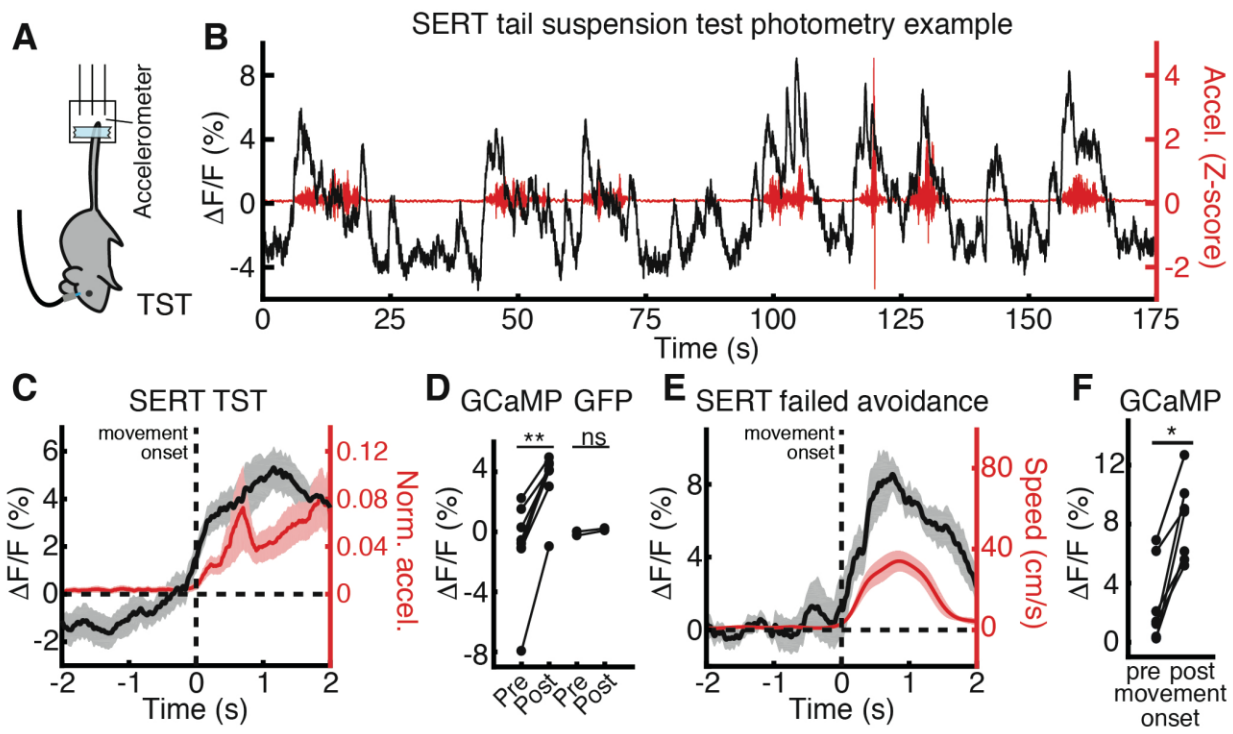

Fig. 2.

DRN 5-HT neural activity increases upon movement in high-threat environments.

(**A**) TST schematic. (**B**) Example TST photometry from the Fig. 1 mouse. GCaMP ΔF/F in black, movement in red. (**C**) Mean ΔF/F aligned to TST movement onset. (**D**) Mean ΔF/F before and after TST movement onset in GCaMP (n=8) and GFP (n=2) mice. (**E**) Mean ΔF/F aligned to escape movement onset during failed avoidance trials. (**F**) Mean ΔF/F before and after escape movement onset in GCaMP (n=7) mice. **P* < 0.05, ***P* < 0.01, Wilcoxon signed-rank test. Error bars indicate s.e.m.

To probe the causal role of DRN 5-HT neurons in regulating movement in different environments, we targeted channelrhodopsin-2(Boyden et al., 2005) to DRN 5-HT neurons via an adeno-associated viral vector (AAV5-EF1□-DIO-ChR2(H134R)-eYFP) injected into the DRN of SERT-Cre mice (Fig. 3A) and implanted an optical fibre over the DRN for light delivery to 5-HT neurons (fig S6A). We then tested mice on the behaviours described above. First, we found that optical stimulation of DRN 5-HT neurons reduced speed in the open field (Fig. 3, B and C, ChR2 3.67+/- 0.31 cm/s versus eYFP 5.16 +/- 0.44 cm/s). We then tested the effects of stimulating DRN 5-HT neurons during the cued approach and avoidance tasks. In both tasks, stimulation began upon auditory cue onset and persisted for 3 seconds regardless of behaviour (fig S6B and D). Speed decreased during stimulation in both tasks (Approach: Fig. 3, D and E, and fig. S6, B and C, ChR2 3.0 +/- 0.3 cm/s versus eYFP 7.1 +/- 1.0 cm/s; Avoidance: Fig. 3, G and H, and fig. S6, D and E, ChR2 2.2 +/- 0.4 cm/s versus eYFP 3.8 +/- 0.4 cm/s), and latency to cross the chamber midline was greater during stimulation in both tasks (Approach: Fig 3I, ChR2 5.3 +/- 0.3 s versus eYFP 3.7 +/- 0.4 s; Avoidance: Fig 3L, ChR2 7.0 +/- 0.3 s versus eYFP 5.7 +/- 0.4 s), consistent with the neural dynamics that we observed in this population (Fig. 1).

When the same mice were subjected to the TST, however, activation of DRN 5-HT neurons instead promoted mobility Fig. 3, J to L). Stimulation provoked an increase in escape-related movements upon light onset, an effect that was not detected in control eYFP-expressing mice. This data is consistent with the increase in DRN 5-HT neural activity observed during escape attempts (Fig. 2), and provides causal evidence for a

switch in DRN 5-HT neuron function from suppression to facilitation of movement in high-threat escape conditions.

The results presented here demonstrate that environmental valence and stress intensity can flip the functional roles of DRN circuits in movement regulation. The notion that movement in states of extreme stress may be differently regulated is not without precedent. Paradoxical kinesia – transient restoration of mobility in emergency situations, such as an earthquake – has been observed in akinetic Parkinsonian patients (Bonanni et al., 2010; Glickstein and Stein, 1991; Souques, 1921) and modelled in rodents(Keefe et al., 1989; Marshall et al., 1976). This phenomenon reveals functional motor programs that reactivate under conditions of high stress, and survives DA antagonism in rodent models (Keefe et al., 1989; Marshall et al., 1976), suggesting alternate regulation. At a more general level, our results reveal that 5-HT function depends on brain state. Clinically, this observation raises the interesting possibility that the impact of 5-HT-targeted therapeutic interventions may depend on brain state; indeed, there is some evidence that therapeutic setting can contribute to the efficacy of 5-HT-targeted pharmacotherapy (Carhart-Harris et al., 2016; Pediatric OCD Treatment Study (POTS) Team, 2004). Computationally, a well-defined role for 5-HT function in the vertebrate forebrain has been more elusive than other neuromodulators, owing to inconsistencies in experimental findings (Dayan and Huys, 2015); accounting for state-dependent function may help to resolve some of these difficulties.

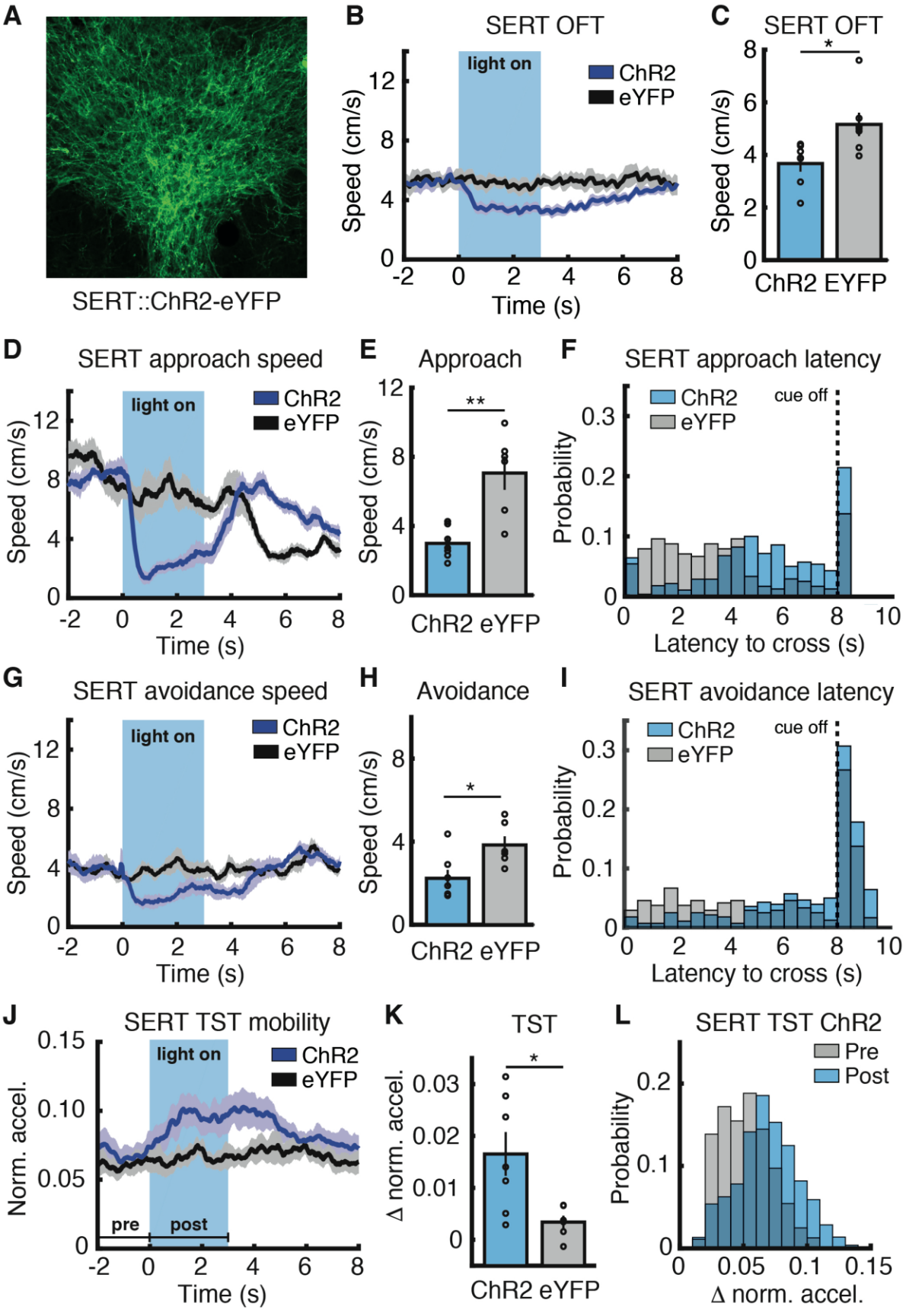
A
SERT::ChR2-eYFP
B
SERT OFT
light on
ChR2
eYFP
Speed (cm/s)
Time (s)
C
SERT OFT
Speed (cm/s)
ChR2 EYFP
D
SERT approach speed
light on
ChR2
eYFP
Speed (cm/s)
Time (s)
E
Approach
Speed (cm/s)
ChR2 eYFP
F
SERT approach latency
ChR2
eYFP
cue off
Probability
Latency to cross (s)
G
SERT avoidance speed
light on
ChR2
eYFP
Speed (cm/s)
Time (s)
H
Avoidance
Speed (cm/s)
ChR2 eYFP
I
SERT avoidance latency
ChR2
eYFP
cue off
Probability
Latency to cross (s)
J
SERT TST mobility
light on
ChR2
eYFP
pre
post
Norm. accel.
Time (s)
K
TST
Δ norm. accel.
ChR2 eYFP
L
SERT TST ChR2
Pre
Post
Probability
Δ norm. accel.

Fig. 3.

DRN 5-HT stimulation suppresses or promotes movement at different threat levels. (**A**) ChR2-eYFP expression in DRN 5-HT neurons in a SERT-Cre mouse. (**B**) Speed aligned to light onset, OFT (SERT::ChR2-eYFP, n=7; SERT::eYFP, n=7). (**C**) Mean speed during stimulation, OFT. (**D**) Speed aligned to light/cue onset, approach task (SERT::ChR2-eYFP, n=7; SERT::eYFP, n=6). (**E**) Mean speed during stimulation, approach task. (**F**) Latency to cross, approach task. $P < 0.0001$, log-rank test. (**G**) Speed aligned to light/cue onset, avoidance task (SERT::ChR2-eYFP, n=7; SERT::eYFP, n=6). (**H**) Mean speed during stimulation, avoidance task. (**I**) Latency to cross distribution, avoidance task. $P < 0.0001$, log-rank test. (**J**) Movement aligned to light onset, TST (SERT::ChR2-eYFP, n=7; SERT::eYFP, n=6). (**K**) Mean difference between pre- and post-light onset movement, TST. (**L**) SERT::ChR2-eYFP movement distribution before and after light onset, TST. $*P < 0.05$, $**P < 0.01$, Wilcoxon rank-sum test. Error bars indicate s.e.m.

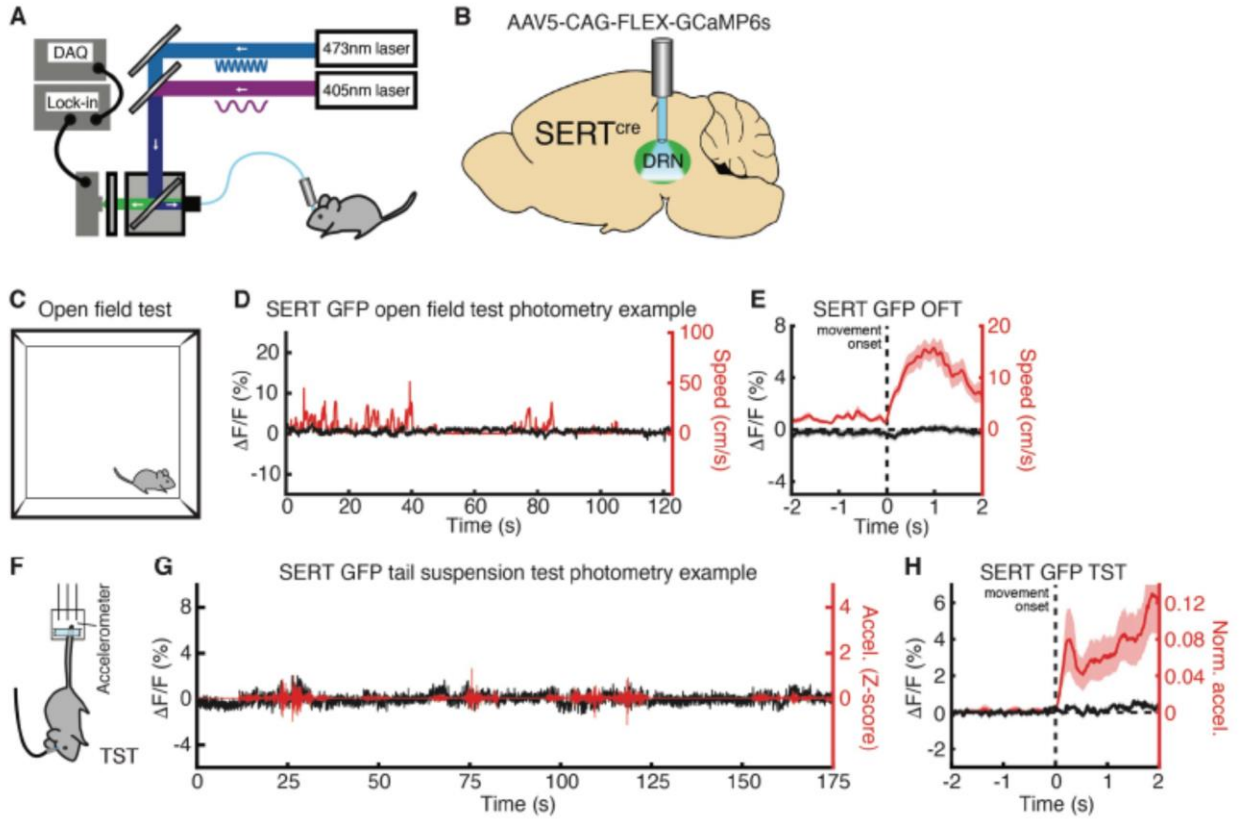

Fig. S1.

(**A**) Fiber photometry schematic. (**B**) Dorsal raphe nucleus (DRN) GCaMP vector and optical fiber placement schematic. (**C**) Open field test (OFT) schematic. (**D**) Example OFT photometry data from a control SERT::GFP mouse. GFP ΔF/F in black, speed in red. (**E**) Mean ΔF/F aligned to OFT movement onset from the same SERT::GFP mouse. (**F**) Tail suspension test (TST) schematic. (**G**) Example TST photometry data from a control SERT::GFP mouse. GFP ΔF/F in black, movement in red. (**H**) Mean ΔF/F aligned to TST movement onset from the same SERT::GFP mouse. X- and Y-axes for all panels match the GCaMP data in the main figures.

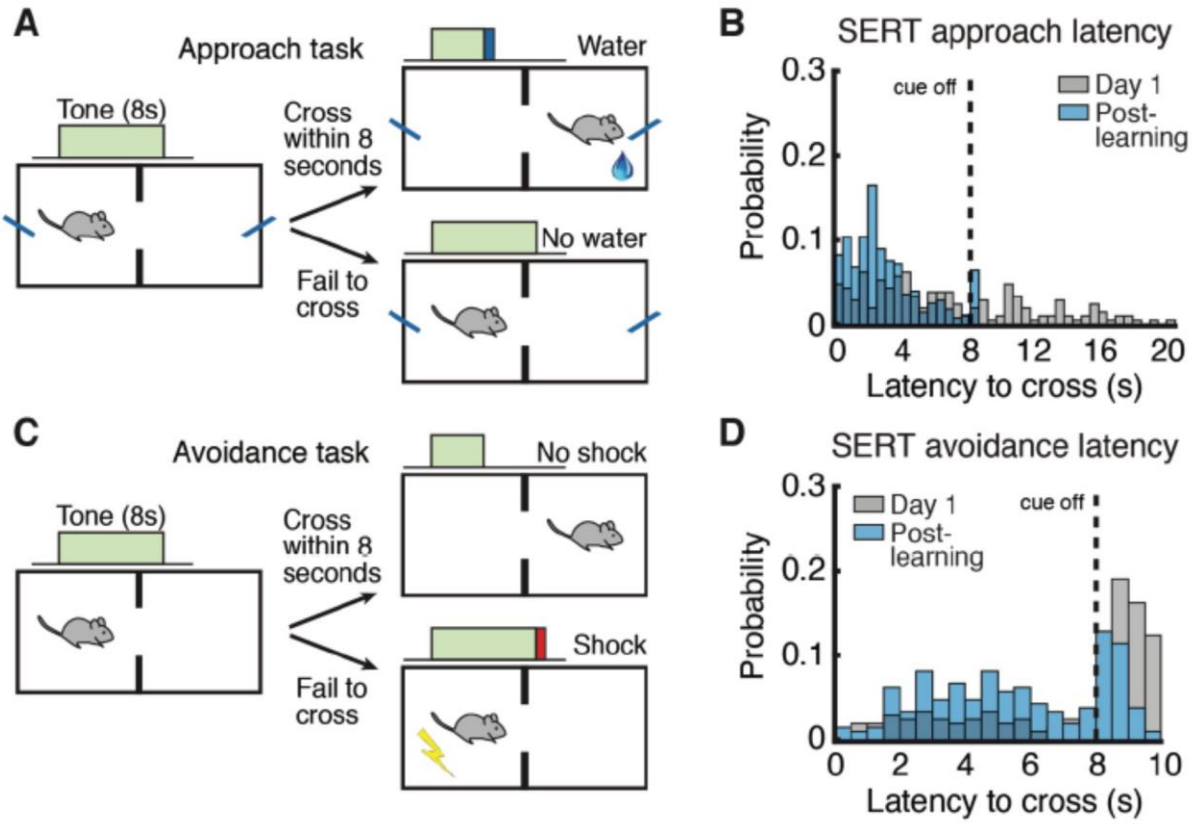

Fig. S2

(**A**) Approach task schematic. (**B**) Latency to cross after cue onset distribution, approach task, day 1 and post-learning (SERT::GCaMP, n=7; *P* < 0.0001, log-rank test). Latency data were not collected for failed approach trials post-learning, but are binned here at 8 s for display only (not for statistical analysis). (**C**) Avoidance task schematic. (**D**) Latency to cross after cue onset distribution, avoidance task, day 1 and post-learning (SERT::GCaMP, n=7; *P* < 0.0001, log-rank test).

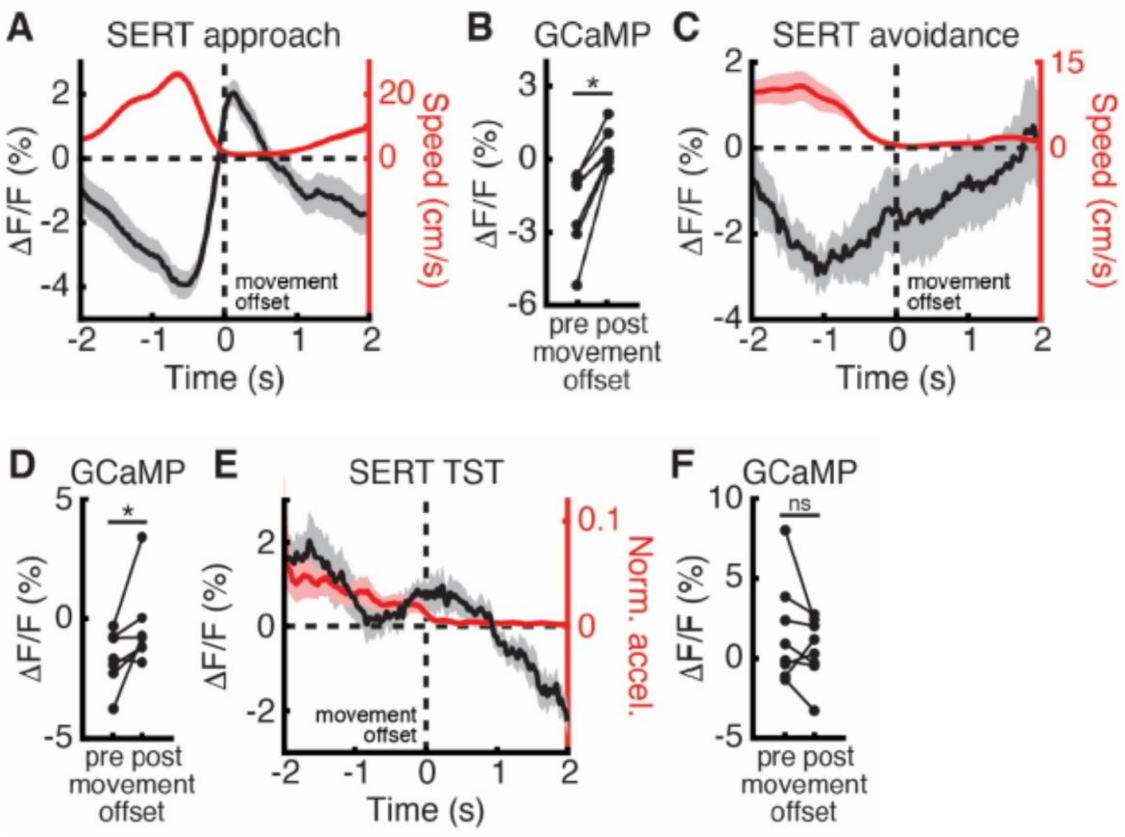

Fig. S3

(**A**) Mean ΔF/F aligned to approach movement offset from a SERT::GCaMP6s mouse. (**B**) Mean ΔF/F before (pre) and after (post) approach movement offset in SERT::GCaMP6s mice (n=7). (**C**) Mean ΔF/F aligned to avoidance movement offset from the mouse in panel A. (**D**) Mean ΔF/F before and after avoidance movement offset (n=7). (**E**) Mean ΔF/F aligned to TST movement offset from the mouse in panel A. (**F**) Mean ΔF/F before and after TST movement offset (n=8). **P* < 0.05, ***P* < 0.01 Wilcoxon signed-rank test. Error bars indicate s.e.m.

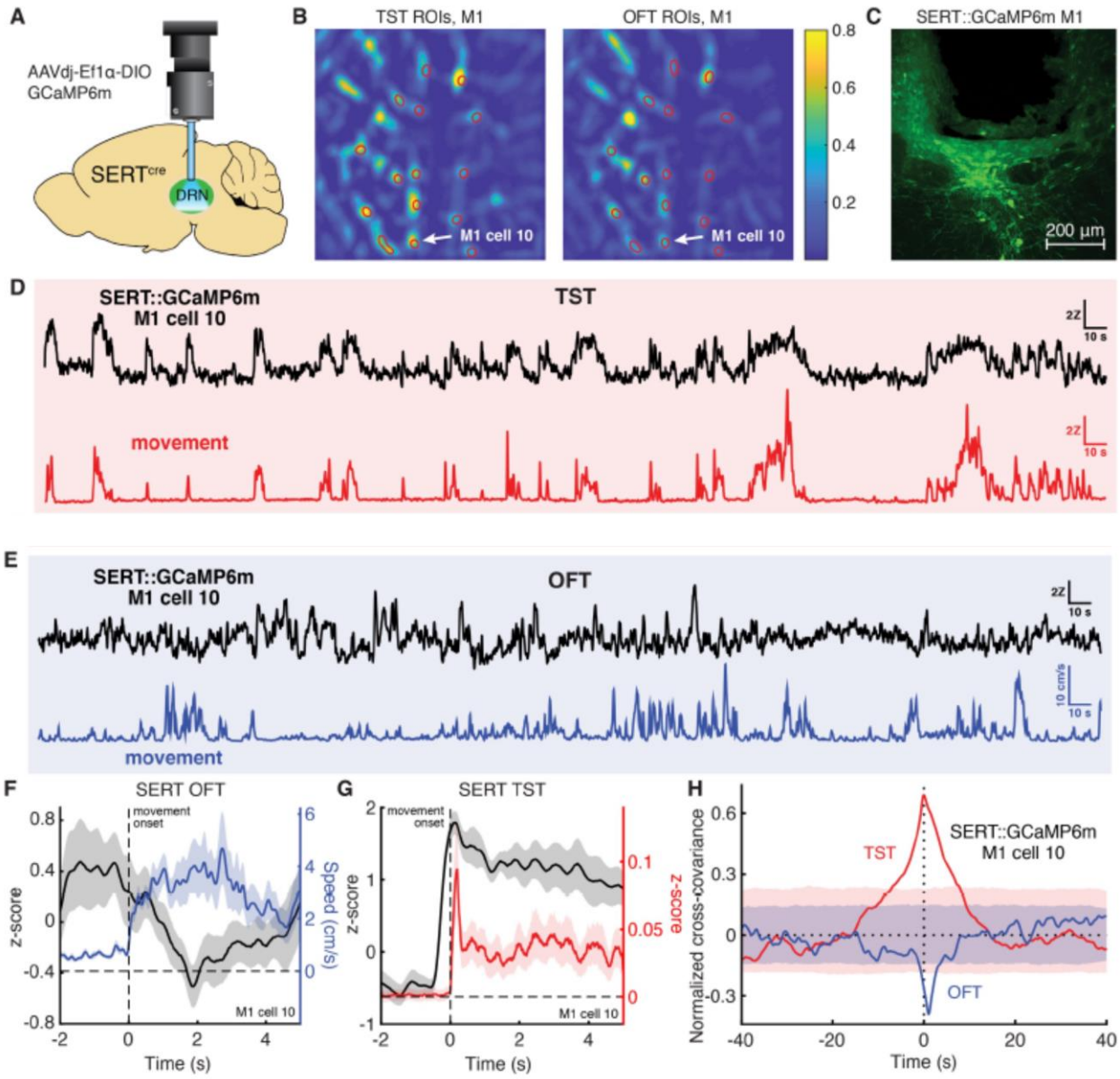

Fig. S4

(A) DRN microendoscopy schematic. (B) MIN1PIPE ROIs, TST and OFT. (C) GCaMP6m expression in mouse M1 DRN 5-HT neurons with GRIN lens track. (D) Example TST microendoscopy data from a mouse M1 DRN 5-HT single neuron. GCaMP activity in black, movement in red. (E) OFT data from the same neuron. GCaMP activity in black, movement in blue. (F) GCaMP6m activity aligned to TST movement onset for the same

neuron. (G) GCaMP6m activity aligned to OFT movement onset for the same neuron. (H) Normalized cross-covariance between GCaMP6m activity and movement for the same neuron in TST (red) and OFT (blue). Light red and blue regions indicate 99% bootstrap confidence intervals. Error bars indicate s.e.m.

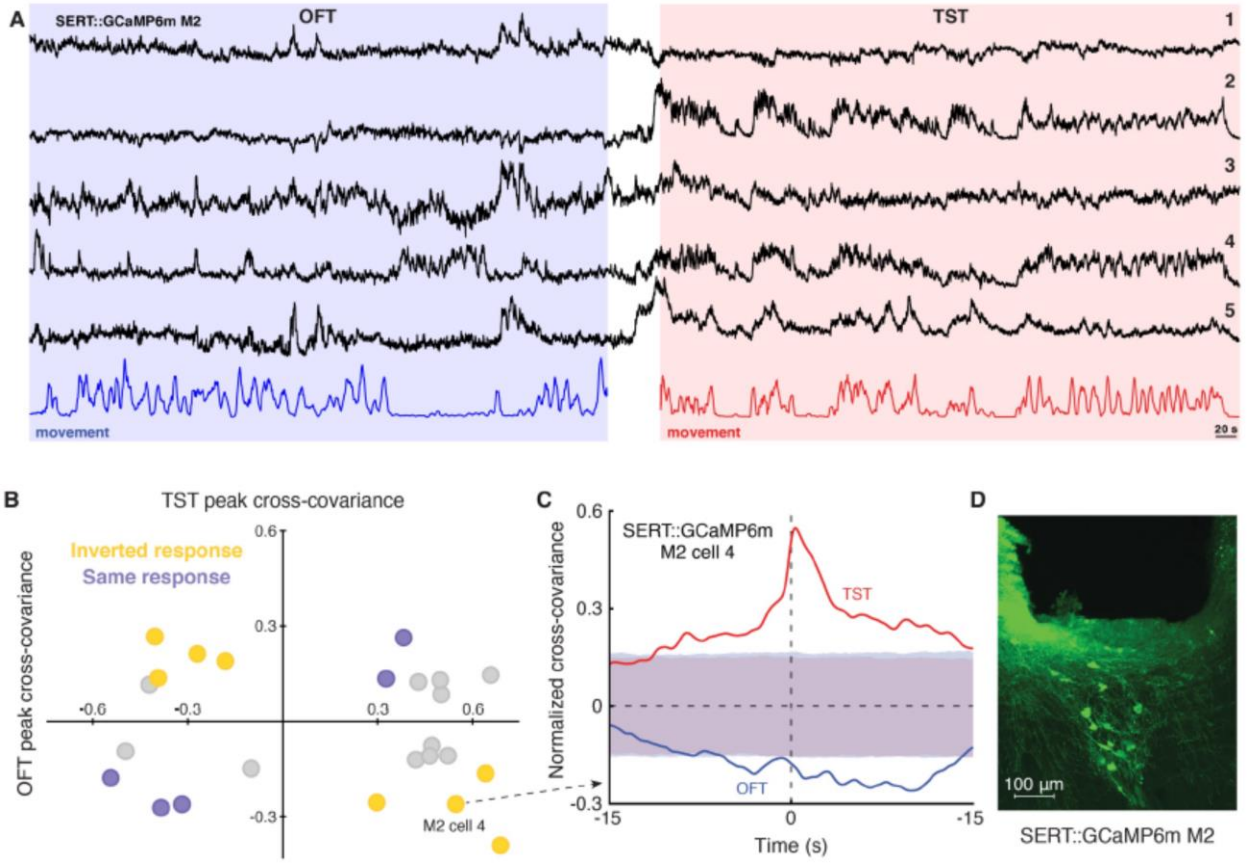

Fig. S5

(**A**) GCaMP6m activity from five DRN 5-HT neurons, continuously recorded during OFT and TST in mouse M2. GCaMP6m activity in black, OFT movement in blue, TST movement in red. (**B**) Peak normalized cross-covariance between movement and neural activity for all recorded DRN 5-HT neurons in OFT and TST environments. Cells with an inverted activity-movement relationship across environments in yellow, cells with the same activity-movement relationship in both environments in purple, cells without a significant movement response in one or both environments in gray. (**C**) Normalized cross-covariance between GCaMP6m activity and movement in TST (red) and OFT (blue) for a mouse M2 neuron. Light red and blue regions indicate 99% bootstrap confidence

intervals. (**D**) GCaMP6m expression in mouse M2 DRN 5-HT neurons with GRIN lens track.

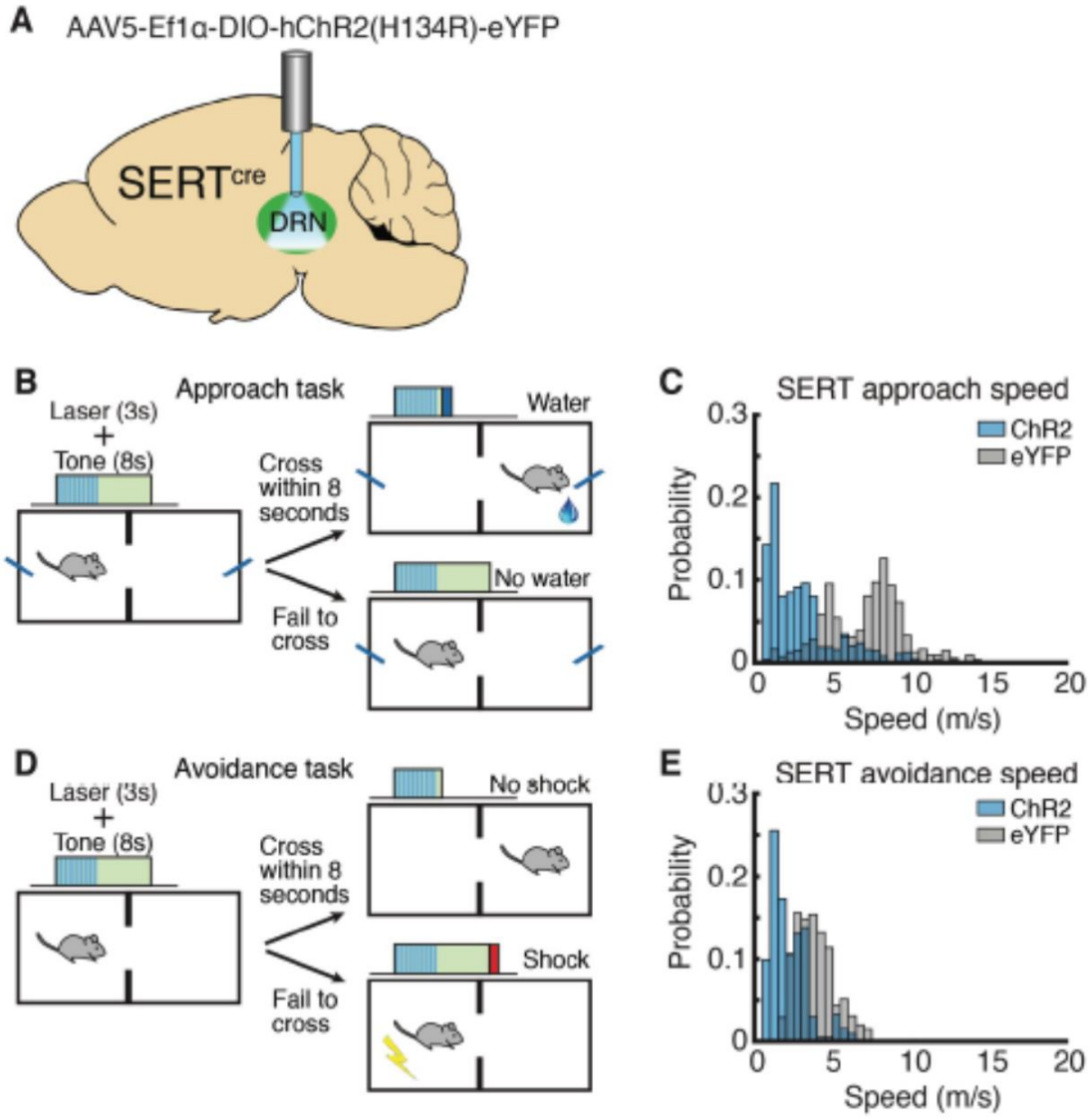

Fig. S6

(**A**) Dorsal raphe nucleus (DRN) ChR2-eYFP vector and optical fiber placement schematic. (**B**) Optogenetic stimulation schematic for approach task. (**C**) Speed distribution during stimulation in approach task (SERT::ChR2-eYFP, n=7; SERT::eYFP, n=6). (**D**) Optogenetic stimulation schematic for avoidance task. (**E**) Speed distribution during stimulation in avoidance task (SERT::ChR2-eYFP, n=7; SERT::eYFP, n=6).

Chapter 3 : Dorsal raphe GABA neuron activity promotes movement in environments with negative valence

The DRN contains a number of distinct cell types in addition to 5-HT neurons(Fu et al., 2010), most prominently a large population of GABAergic neurons that has been shown to synapse onto DRN 5-HT neurons (Zhou et al., 2017). DRN GABA neurons have been implicated in aggression and the acquisition of social avoidance (Challis et al., 2013; Takahashi et al., 2010) and may play a role in the protective effect of behavioural control over stressors (Maier and Watkins, 2005). These neurons receive afferents from cortical and subcortical regions that provide information about environmental context and internal state (Celada et al., 2001; Jankowski and Sesack, 2004; Zhou et al., 2017), and also receive a direct glutamatergic input from the retina necessary for looming-evoked escape responses (Huang et al., 2017).

We utilized fiber photometry (Cui et al., 2013; Gunaydin et al., 2014) to monitor the real-time neural dynamics of genetically defined DRN GABA neurons during movement in freely behaving mice. We injected Cre-dependent AAV-GCaMP6s (Chen et al., 2013) into the DRN of Vgat-ires-Cre mice (Vong et al., 2011) to target expression to GABA neurons, and implanted an optical fibre over the DRN (fig. S7, A and B, and fig. S8).

We recorded DRN GABA neural activity while mice engaged in the cued approach and avoidance behaviours described above (Fig. 1). Intriguingly, we found that DRN GABA activity decreased during movement to obtain a reward in the cued approach task

(Fig. 4, A to C; movement offset, fig. S3, G and H) but increased during movement to avoid a shock in the cued avoidance task (Fig. 4, F to H; movement offset, fig. S3, I and J), unlike the decrease in activity observed during both behaviours in DRN 5-HT neurons (Fig. 1).

We examined the timing of the neural response inversion in DRN GABA neurons as mice transitioned between positive and negative environments. In our experiments, mice first received extensive training in the approach task, during which DRN GABA neuron data was recorded daily, then mice were trained on the avoidance task. Before the first ever CS-US aversive pairing, mice were allowed to freely explore the operant chamber for several minutes while DRN GABA neuron activity was recorded (mice likely recognized this chamber as a positive environment, as it was where approach conditioning took place). Recordings continued during avoidance training on this day and subsequent days. We were thus able to examine the within-session timing of the shift in movement-related DRN GABA dynamics following the first shock exposure. DRN GABA activity, on average, inverted following exposure to two shocks (some mice showed inversion after the first shock), and reached peak inversion following exposure to four shocks (fig. S9 and fig. S10). Although overt behavioral requirements are similar in these two tasks, reward and punishment tasks differ in environmental valence (Cohen et al., 2015a; Hayashi et al., 2015), a factor that may contribute to the distinct neural dynamics observed during movement.

In order to test this hypothesis, we recorded DRN GABA neural activity while mice engaged in wheel running (Fig. 4k), a voluntary behavior that can function as a primary reinforcer (Greenwood et al., 2011; Sherwin, 1998). Much like movement to obtain reward in the approach task, running bouts on the wheel were associated with a reduction in DRN GABA activity (Fig. 4, L to N; GFP data, Fig. 4N and fig. S7, C to E). We then recorded DRN GABA neural activity while mice engaged in the TST, which can induce depression-like behavioural changes (Strekalova et al., 2004), and discovered that active escape behaviours were correlated with a robust increase in the DRN GABA fluorescence signal (Fig. 4, P to S, movement offset fig. S3, K and L), an effect that was not detected in control GFP-expressing mice (Fig. 4S and fig. S7, F to H). Consistent with this finding, DRN GABA neural activity increased on movement in escape (failed) trials in the avoidance task (fig. S7, I to L). Thus, in rewarding environments movement and DRN GABA neural activity are inversely correlated, but in aversive environments they are directly correlated, findings consistent with a role for environmental valence in shaping the movement-related dynamics of this neural population.

Finally, we investigated if DRN GABA neurons have a causal role in the regulation of movement, and if this role depends on environmental valence. We injected AAV5-EF1a-DIO-ChR2(H134R)-eYFP into the DRN of Vgat-ires-Cre mice, and implanted an optical fibre over the DRN for light delivery and stimulation of DRN GABA neural activity (fig. S11, A and B). Mice were trained on the cued approach task (Fig. 1), and the impact of stimulation on speed and latency from cue onset to chamber crossing was measured. Even though the mice tested in these experiments were the same as those used in the

following cued avoidance and TST experiments, stimulation of GABA DRN neurons had no impact on either velocity (Fig. 4, D and E, and fig. S11 ChR2 7.3 +/- 0.7 m/s versus eYFP 6.7 +/- 1.0 m/s) or latency to chamber crossing (fig. S11E, ChR2 3.5 +/- 0.3 s versus eYFP 3.5 +/- 0.3 s) in the cued approach task. Similarly, stimulating this neural population had no impact on wheel mobility (Fig. 4O). This effect was not simply due to physical limitations on movement, as stimulation facilitated higher mean and peak velocities in the open field (fig. S12).

We then trained these mice on the cued avoidance task (Fig. 1), and assessed the impact of stimulation on movement. ChR2-eYFP mice showed increased speed (Fig. 4, I and J and fig. S11, F and G. ChR2 7.7 +/- 0.7 m/s versus eYFP 4.0 +/- 0.2 m/s) and reduced latency to avoidance (fig.S11H, 4.1 +/- 0.37 s vs 5.6 +/- 0.19 s) during light stimulation compared to control eYFP mice. Likewise, stimulation increased struggling behaviour in the TST compared to control eYFP mice (Fig. 4T), results consistent with the movement-related increase in neural activity observed during cued avoidance and the TST. These data reveal that DRN GABA neurons play a specialized causal role in promoting movement in environments with negative valence, facilitating actions to avoid and escape threats(Huang et al., 2017).

DRN 5-HT and GABA neurons receive distinct distributions of long-range afferents (Weissbourd et al., 2014), which include GABAergic inputs from regions including the central amygdala and hypothalamus – these differences alone may account for 5-HT and GABA differential response properties. Second, the population of GABA neurons within

the DRN is diverse and includes subpopulations that are differentially connected to DRN 5-HT neurons. Weissbourd et al. used rabies tracing to demonstrate that DRN 5-HT neurons receive enriched local GABAergic input from the adjacent midbrain reticular nucleus (MRtN) and reduced local input from the DRN lateral wings (fig. S14A). Interestingly, during experiments to characterize GABAergic subtypes within the DRN, we found an anatomical segregation of local somatostatin (SST), parvalbumin (PV), and vasoactive intestinal peptide (VIP) neurons corresponding to these regions – SST neurons were located in the lateral wings of the DRN, PV neurons were located in the immediately adjacent MRtN, and VIP neurons were located at the top edge of the DRN (fig. S14, B, C, and K):

We hypothesized that DRN SST neurons may be the primary GABAergic population active during TST movements, since weak connectivity between this lateral wing population and DRN 5-HT neurons would permit 5-HT neurons to respond as well, and that more strongly connected MRtN PV neurons may show movement-related inhibition compatible with DRN 5-HT neuron activation during TST movements. To test this hypothesis, we probed the movement-related neural dynamics of these populations with fiber photometry. Contrary to our hypothesis, we found that both SST and PV neural populations responded vigorously during escape movements in the TST (fig. S14, D to J). Although VIP neurons did not specifically respond during movements this population was suppressed strongly following shock exposure, suggesting a potential role in shaping environment-dependent DRN activity (fig. S14, L and M).

The response properties of a neuron depend on the combination of inputs and their temporal and spatial distribution – it is unlikely that inhibitory input onto a cell, even strong inhibition, will always simply shut down the target. Inhibition can be utilized for other computational purposes, and evidence for GABAergic shaping of temporal patterns of activity has been obtained in several different brain regions (e.g. Pouille and Scanziani, 2001; Sohal et al., 2009). The VTA, a neuromodulatory region with similar local GABA inhibition, also exhibits distinct dynamics in its principal output neurons and GABA neurons – VTA DA neurons respond phasically to positive reward prediction error, while VTA GABA neurons show a prolonged tonic response to the same stimulus (Cohen et al., 2012). We suspect that this aspect of GABA neuron function is more likely to be the rule than the exception, and thus we hypothesize that temporal shaping of the DRN 5-HT neural response may be a major function of local GABAergic input. There may be an additional computational advantage to this finding. DRN GABA neurons, like DRN 5-HT neurons, project widely to target regions that include the lateral hypothalamus and the nucleus accumbens (Bang and Commons, 2012). Valence-dependent movement encoding in DRN GABA neurons combined with threat-dependent movement encoding in DRN 5-HT neurons conveys more information than either signal alone, and this combination may be utilized by downstream regions to more finely gauge environmental quality.

Here, we have probed the neural dynamics and functional roles of DRN neural circuits in the regulation of movement, using optical methods for the readout and control of neural activity in two genetically distinct DRN cell types. We have demonstrated that

intense environmental stress switches DRN 5-HT neurons from inhibition of movement to facilitation, and that DRN GABA neurons selectively facilitate movement in negatively-valenced environments, consistent with the observed state-dependent neural dynamics of both cell types. These results reveal a critical role for DRN circuits in state-dependent behavioural suppression or activation and suggest that a primary DRN function may be to promote an adaptive, context-dependent level of behavioural activity.

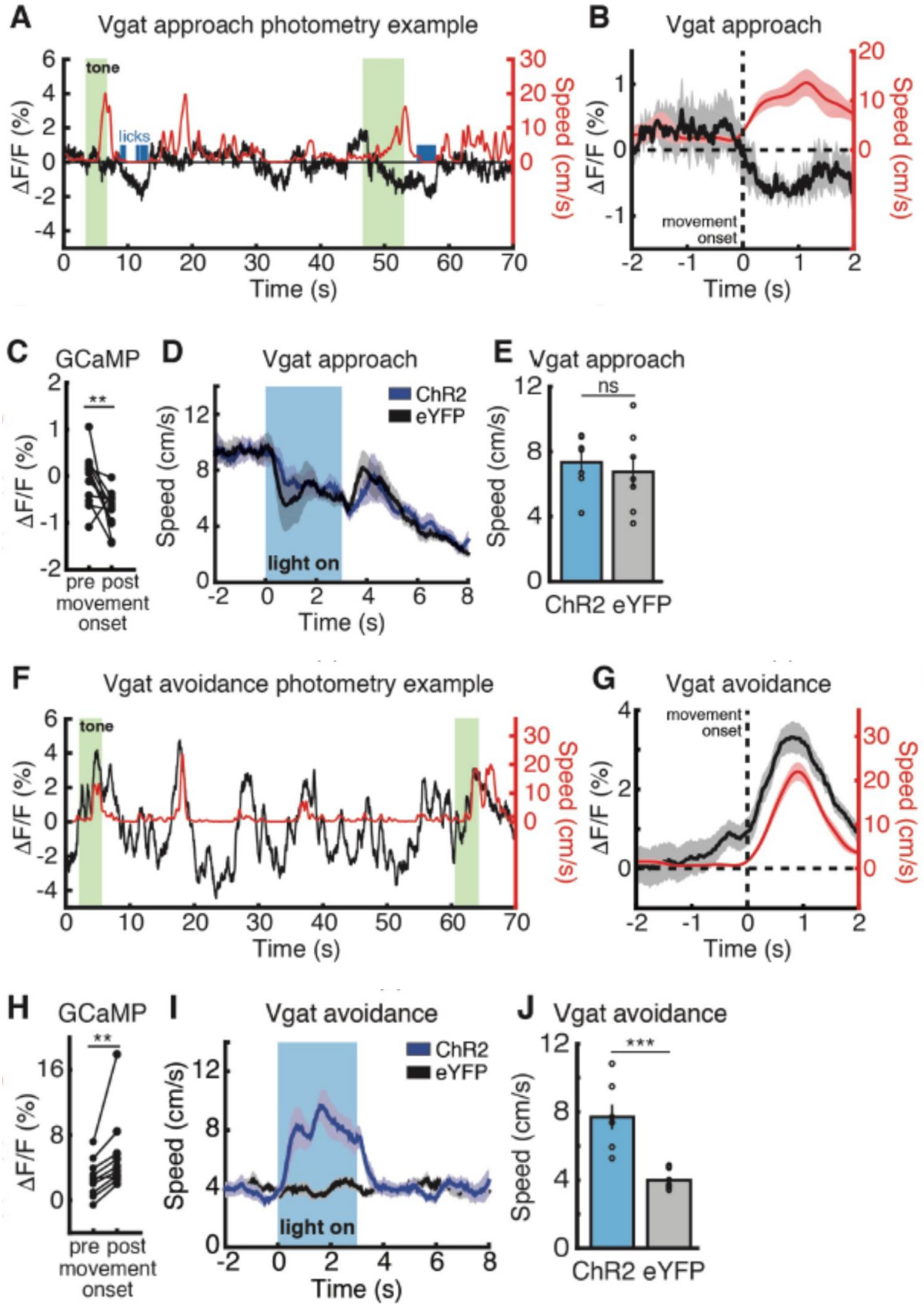
A
Vgat approach photometry example
tone
licks
ΔF/F (%)
Speed (cm/s)
Time (s)
B
Vgat approach
movement onset
C
GCaMP
**
pre post
movement onset
D
Vgat approach
ChR2
eYFP
light on
E
Vgat approach
ns
ChR2 eYFP
F
Vgat avoidance photometry example
G
Vgat avoidance
H
GCaMP
I
Vgat avoidance
J
Vgat avoidance
***

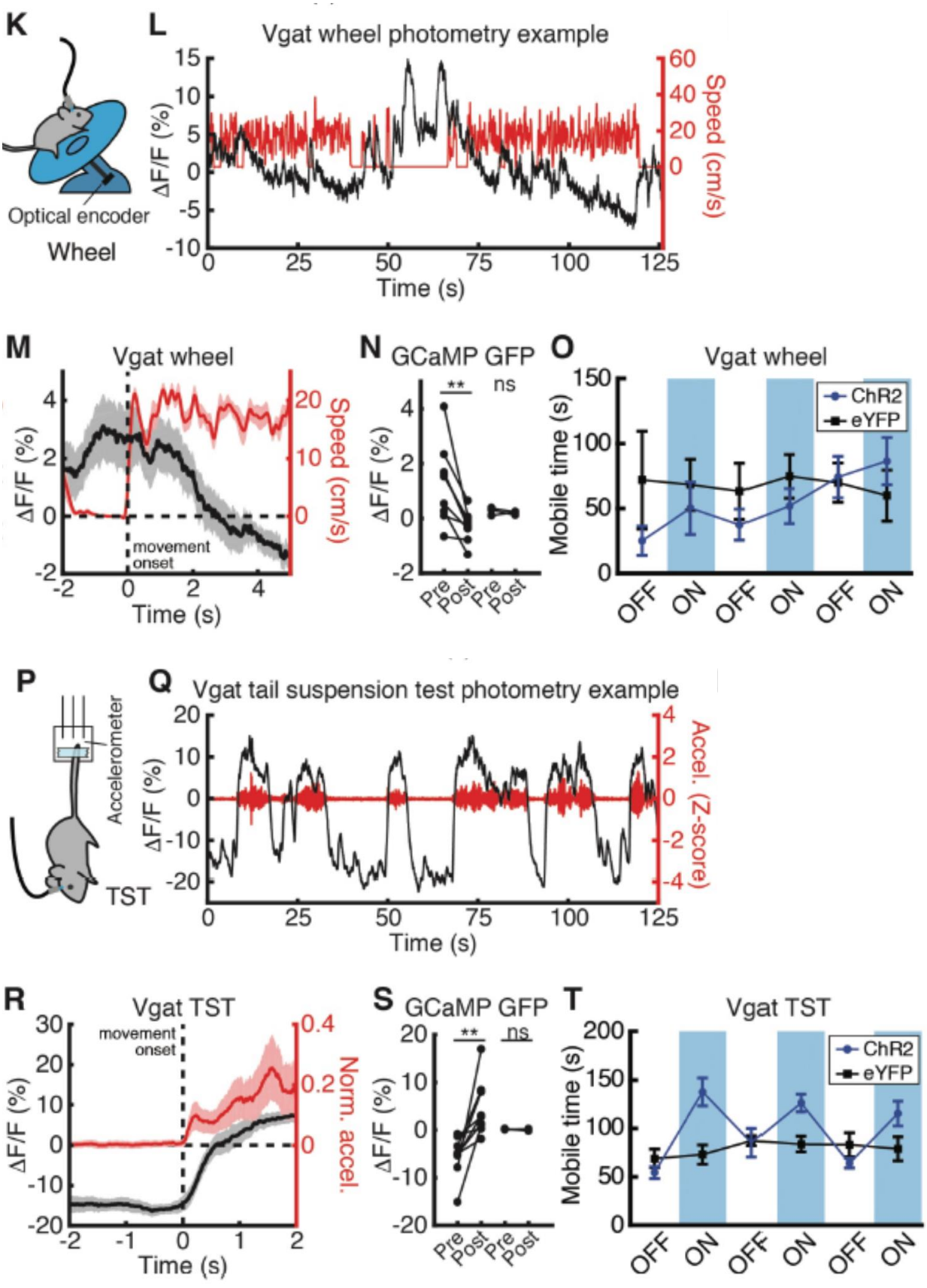
K
Optical encoder
Wheel
L
Vgat wheel photometry example
ΔF/F (%)
Speed (cm/s)
Time (s)
M
Vgat wheel
movement onset
ΔF/F (%)
Speed (cm/s)
Time (s)
N
GCaMP GFP
**
ns
ΔF/F (%)
Pre
Post
Pre
Post
O
Vgat wheel
Mobile time (s)
ChR2
eYFP
OFF
ON
OFF
ON
OFF
ON
P
Accelerometer
TST
Q
Vgat tail suspension test photometry example
ΔF/F (%)
Accel. (Z-score)
Time (s)
R
Vgat TST
movement onset
ΔF/F (%)
Norm. accel.
Time (s)
S
GCaMP GFP
**
ns
ΔF/F (%)
Pre
Post
Pre
Post
T
Vgat TST
Mobile time (s)
ChR2
eYFP
OFF
ON
OFF
ON
OFF
ON

Fig. 4.

DRN GABA stimulation promotes movement in environments with negative valence.

(**A**) Approach photometry example from a Vgat::GCaMP6s mouse. GCaMP ΔF/F in black, speed in red. (**B**) Mean ΔF/F aligned to approach movement onset. (**C**) Mean ΔF/F before and after approach movement onset (n=11). (**D**) Speed aligned to stimulation/cue onset, approach (Vgat::ChR2-eYFP, n=8; Vgat::eYFP, n=7). (**E**) Mean speed during stimulation, approach. (**F**) Example avoidance photometry. (**G**) Mean ΔF/F aligned to avoidance movement onset. (**H**) Mean ΔF/F before and after avoidance movement onset (n=10). (**I**) Speed aligned to stimulation/cue onset, avoidance (Vgat::ChR2-eYFP, n=8; Vgat::eYFP, n=7). (**J**) Mean speed during stimulation, avoidance. (**K**) Wheel schematic. (**L**) Example wheel photometry. (**M**) Mean ΔF/F aligned to wheel movement onset. (**N**) Mean ΔF/F before and after wheel movement onset in GCaMP (n=9) and GFP (n=3) mice. (**O**) Mean mobile time in 3-minute stimulation or non-stimulation blocks, wheel (Vgat::ChR2-eYFP, n=7; Vgat::eYFP, n=7; $P = 0.9015$, Wilcoxon rank-sum test). (**P**) TST schematic. (**Q**) TST photometry example. (**R**) Mean ΔF/F aligned to TST movement onset. (**S**) Mean ΔF/F before and after TST movement onset in GCaMP (n=9) and GFP (n=3) mice. (**T**) Mean mobile time in 3-minute stimulation or non-stimulation blocks, TST (Vgat::ChR2-eYFP, n=7; Vgat::eYFP, n=7; $P = 0.007$, Wilcoxon rank-sum test). $^{**}P < 0.01$, $^{***}P < 0.001$ Wilcoxon signed-rank test (photometry) or Wilcoxon rank-sum test (optogenetics). Error bars indicate s.e.m.

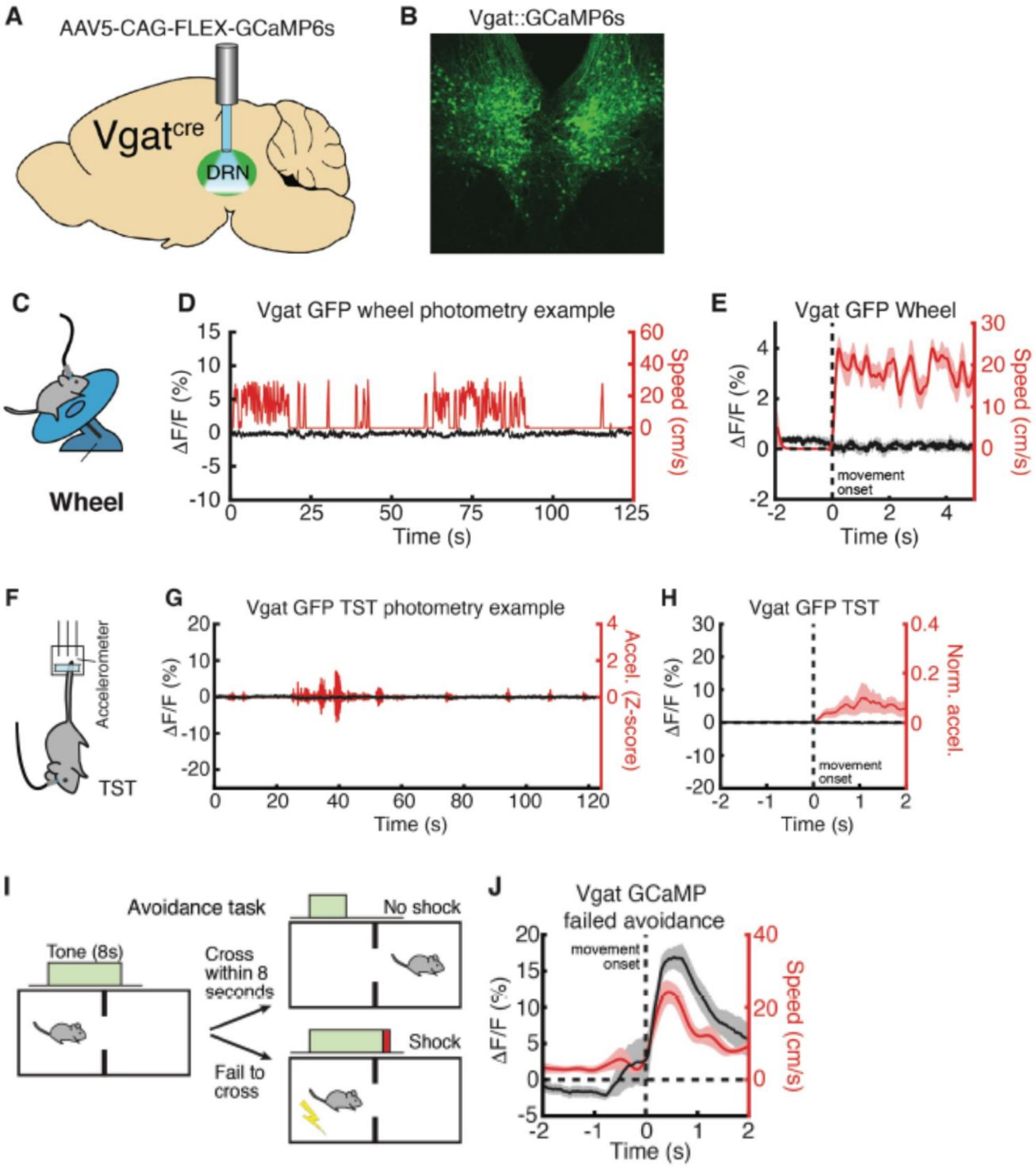
A
AAV5-CAG-FLEX-GCaMP6s
Vgat^cre
DRN
B
Vgat::GCaMP6s
C
Wheel
D
Vgat GFP wheel photometry example
ΔF/F (%)
Speed (cm/s)
Time (s)
E
Vgat GFP Wheel
movement onset
F
Accelerometer
TST
G
Vgat GFP TST photometry example
Accel. (Z-score)
H
Vgat GFP TST
Norm. accel.
I
Avoidance task
Tone (8s)
Cross within 8 seconds
No shock
Shock
Fail to cross
J
Vgat GCaMP failed avoidance

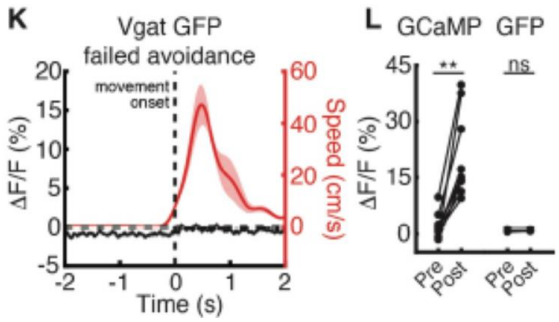

Fig. S7

(**A**) Dorsal raphe nucleus (DRN) viral vector and optical fiber placement schematic. (**B**) GCaMP6s expression in DRN GABA neurons in a Vgat-Cre mouse. (**C**) Wheel schematic. (**D**) Example wheel photometry data from a Vgat::GFP mouse. GFP ΔF/F in black, speed in red. (**E**) Mean ΔF/F aligned to wheel movement onset from the same mouse. (**F**) Tail suspension test (TST) schematic. (**G**) Example TST photometry data from a Vgat::GFP mouse. (**H**) Mean ΔF/F aligned to TST movement onset from the same mouse. (**I**) Avoidance task schematic. (**J**) Mean ΔF/F aligned to escape movement onset during failed avoidance trials from a Vgat::GCaMP6s mouse. (**K**) Mean ΔF/F aligned to escape movement onset during failed avoidance trials from a Vgat::GFP mouse. (**L**) Mean ΔF/F before and after movement onset to escape the shock in GCaMP (n=10) and GFP (n=3) mice. ***P* < 0.01, Wilcoxon signed-rank test. Error bars indicate s.e.m.

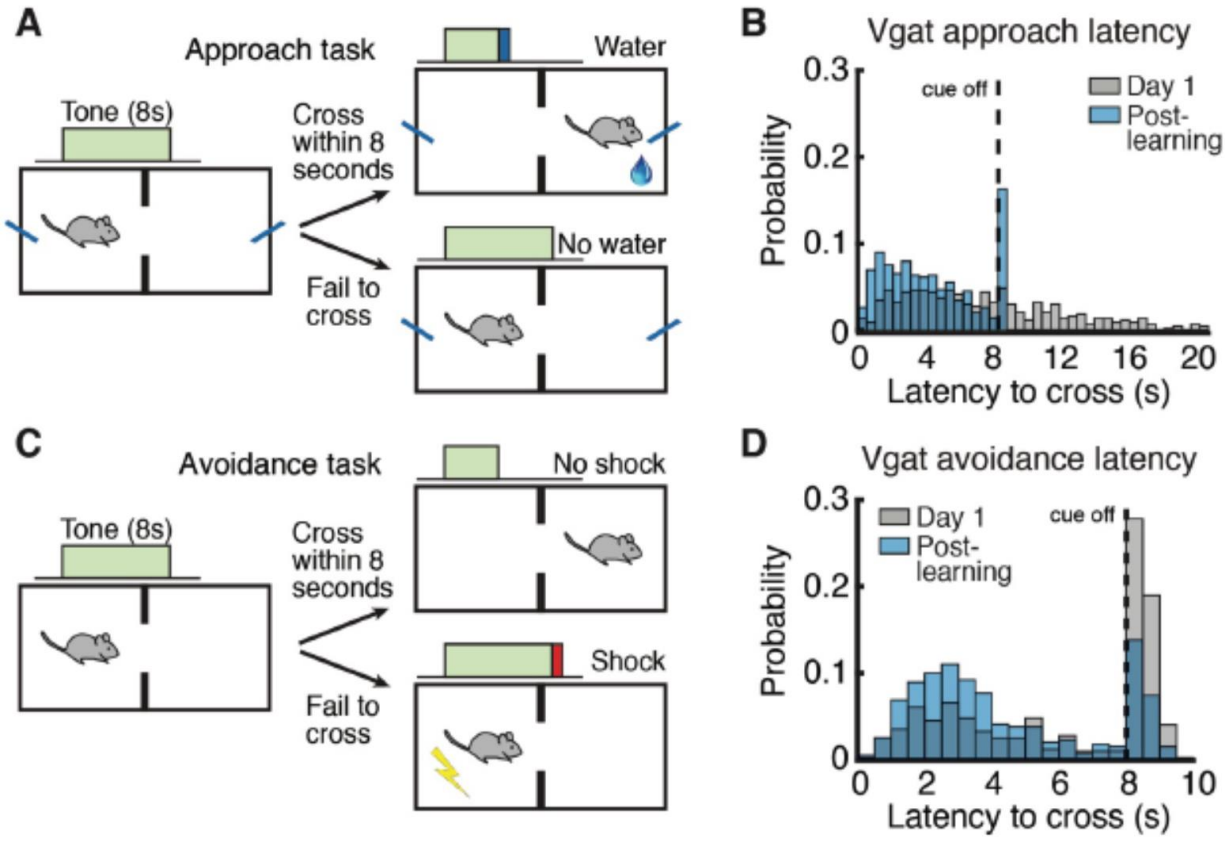

Fig. S8

(**A**) Approach task schematic. (**B**) Latency to cross after cue onset distribution, approach task, day 1 and post-learning (Vgat::GCaMP, n=11; $P < 0.0001$, log-rank test). Latency data were not collected for failed approach trials post-learning, but are binned here at 8 s for display only (not for statistical analysis). (**C**) Avoidance task schematic. (**D**) Latency to cross after cue onset distribution, avoidance task, day 1 and post-learning (Vgat::GCaMP, n=10; $P < 0.0001$, log-rank test).

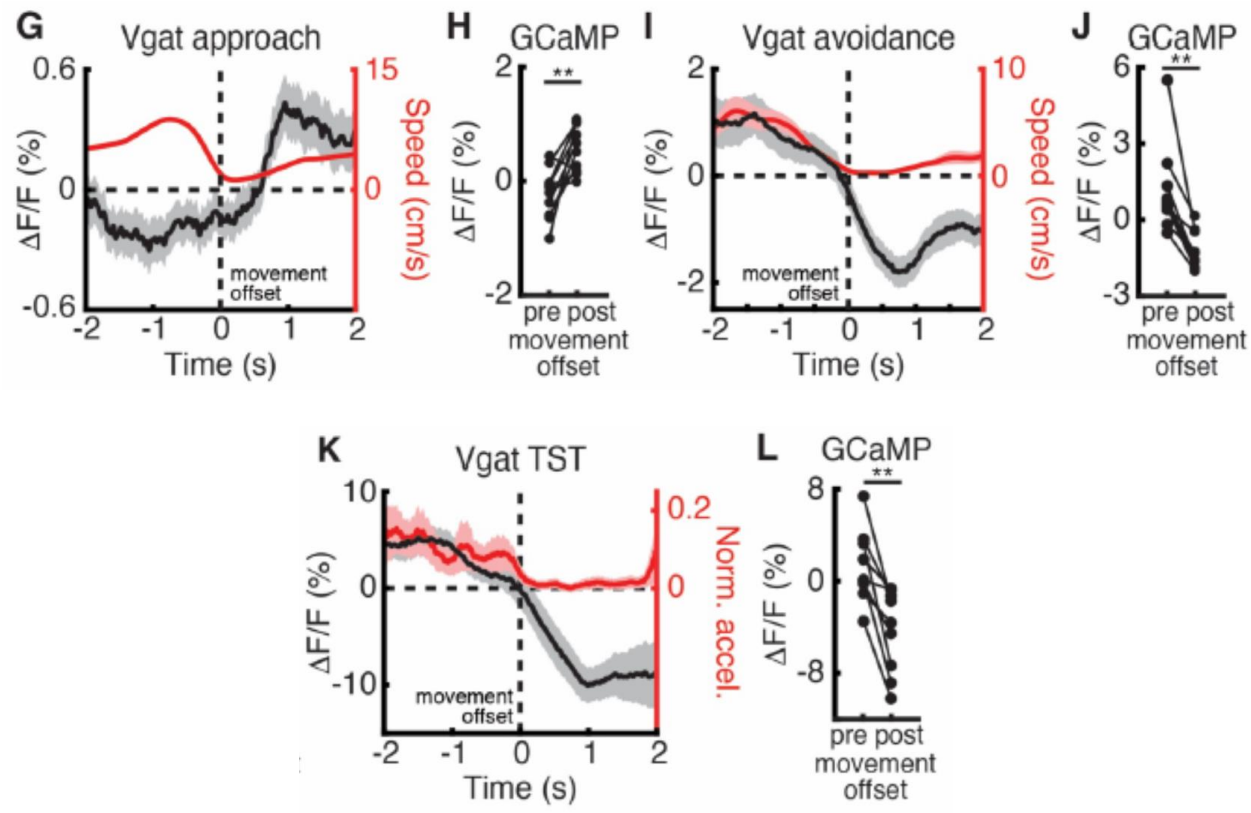

Fig. S9

(**G**) Mean ΔF/F aligned to approach movement offset from a Vgat::GCaMP6s mouse. (**H**) Mean ΔF/F before and after approach movement offset in Vgat::GCaMP6s mice (n=11). (**I**) Mean ΔF/F aligned to avoidance movement offset from the mouse in panel G. (**J**) Mean ΔF/F before and after avoidance movement offset (n=10). (**K**) Mean ΔF/F aligned to TST movement offset from the mouse in panel G. (**L**) Mean ΔF/F before and after TST movement offset (n=9) mice. **P* < 0.05, ***P* < 0.01 Wilcoxon signed-rank test. Error bars indicate s.e.m.

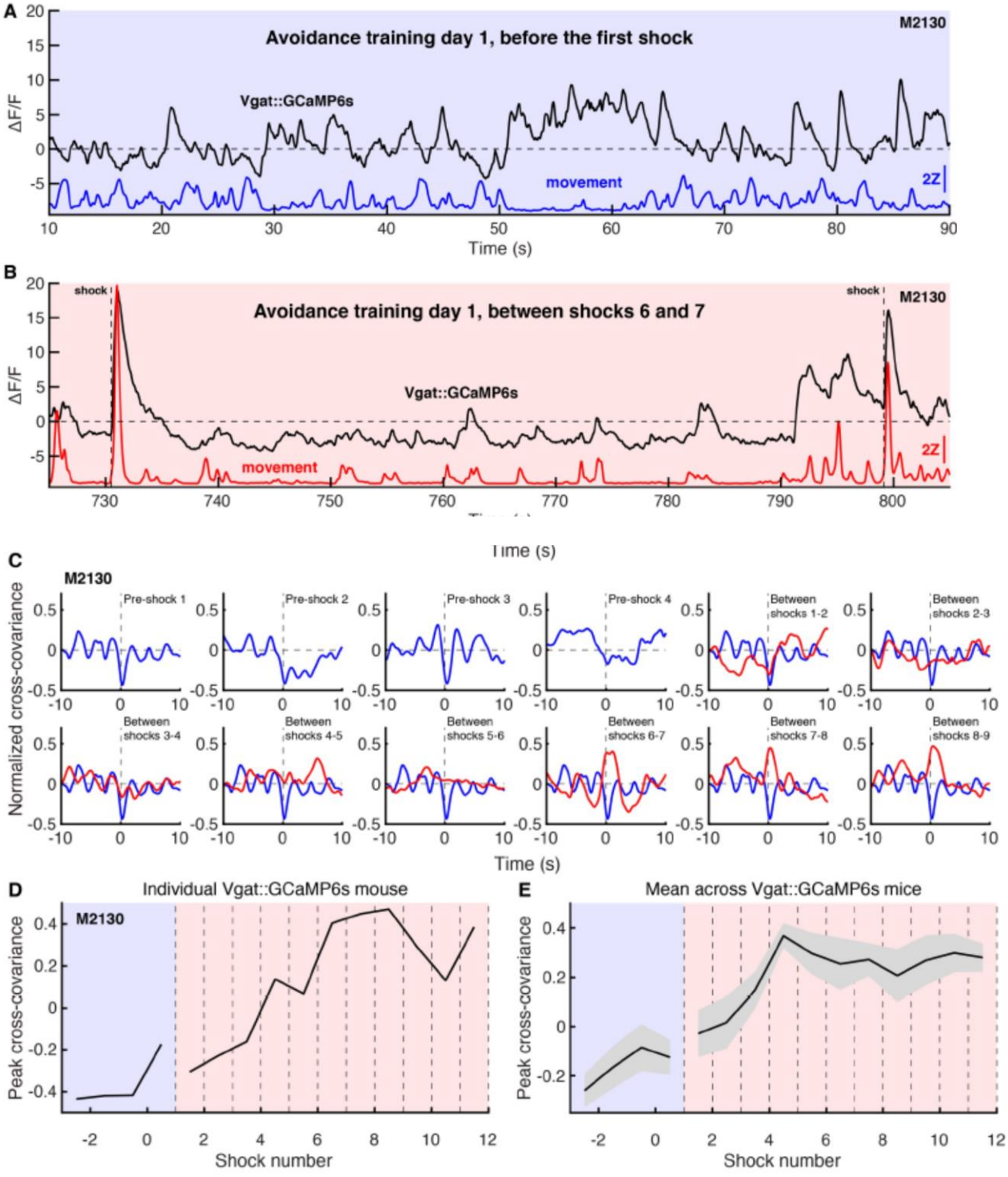
A
Avoidance training day 1, before the first shock
M2130
Vgat::GCaMP6s
movement
2Z
ΔF/F
Time (s)
B
Avoidance training day 1, between shocks 6 and 7
shock
shock
M2130
Vgat::GCaMP6s
movement
2Z
ΔF/F
Time (s)
C
M2130
Pre-shock 1
Pre-shock 2
Pre-shock 3
Pre-shock 4
Between shocks 1-2
Between shocks 2-3
Between shocks 3-4
Between shocks 4-5
Between shocks 5-6
Between shocks 6-7
Between shocks 7-8
Between shocks 8-9
Normalized cross-covariance
Time (s)
D
Individual Vgat::GCaMP6s mouse
M2130
Peak cross-covariance
Shock number
E
Mean across Vgat::GCaMP6s mice
Peak cross-covariance
Shock number

Fig. S10

(**A**) Example pre-shock photometry data from a Vgat::GCaMP6s mouse. GCaMP6s ΔF/F in black, speed in blue. (**B**) Example photometry data from the mouse in panel A following 6 shocks. GCaMP6s ΔF/F in black, speed in red. (**C**) Normalized cross-covariance between movement and GCaMP6s ΔF/F from the mouse in panel A during successive epochs of time. Pre-shock cross-covariance in blue, post-shock cross-covariance in red. Panels 5-12 include pre-shock panel 1 cross-covariance for comparison. (**D**) Peak cross-covariance during successive epochs from the same mouse. (**E**) Mean peak cross-covariance during successive epochs across mice. Error bars indicate s.e.m.

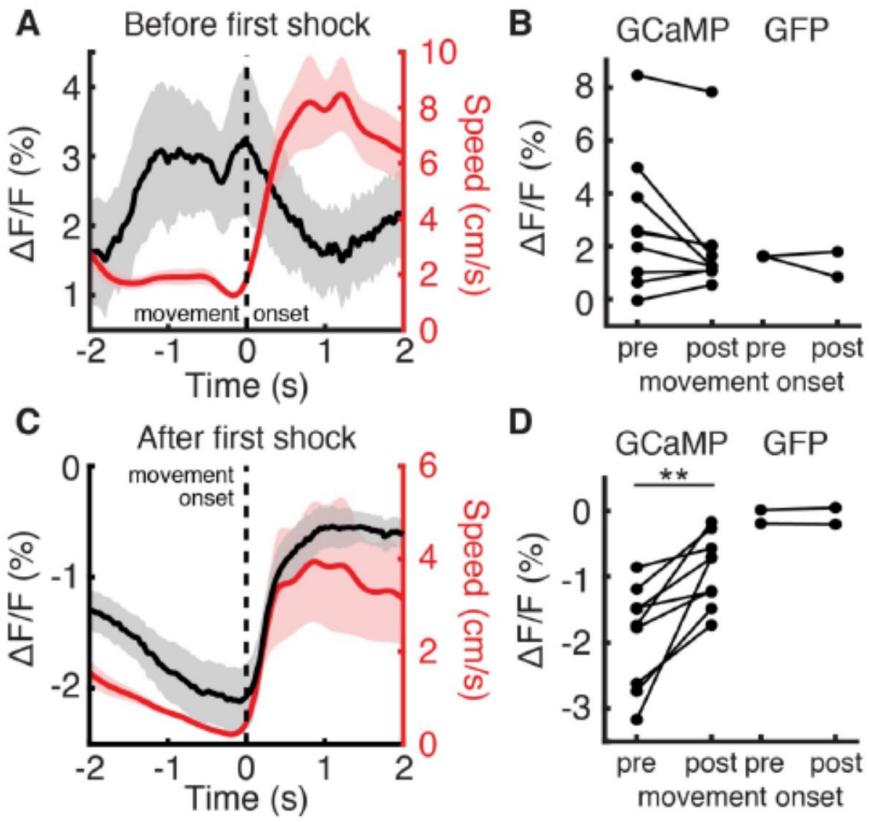

Fig. S11

(**A**) Mean DRN ΔF/F from a Vgat::GCaMP6s mouse aligned to movement onset, day 1 of avoidance training, before first shock. GCaMP ΔF/F in black, speed in red. (**B**) Mean ΔF/F before (pre) and after (post) movement onset in GCaMP (n=9) and GFP (n=2) mice, day 1 of avoidance training before first shock. (**C**) Mean ΔF/F aligned to movement onset from the mouse in panel A, same day after the first shock. (**D**) Mean ΔF/F before and after movement onset after the first shock in GCaMP (n=9) and GFP (n=2) mice. ***P* < 0.01, Wilcoxon signed-rank test. Error bars indicate s.e.m.

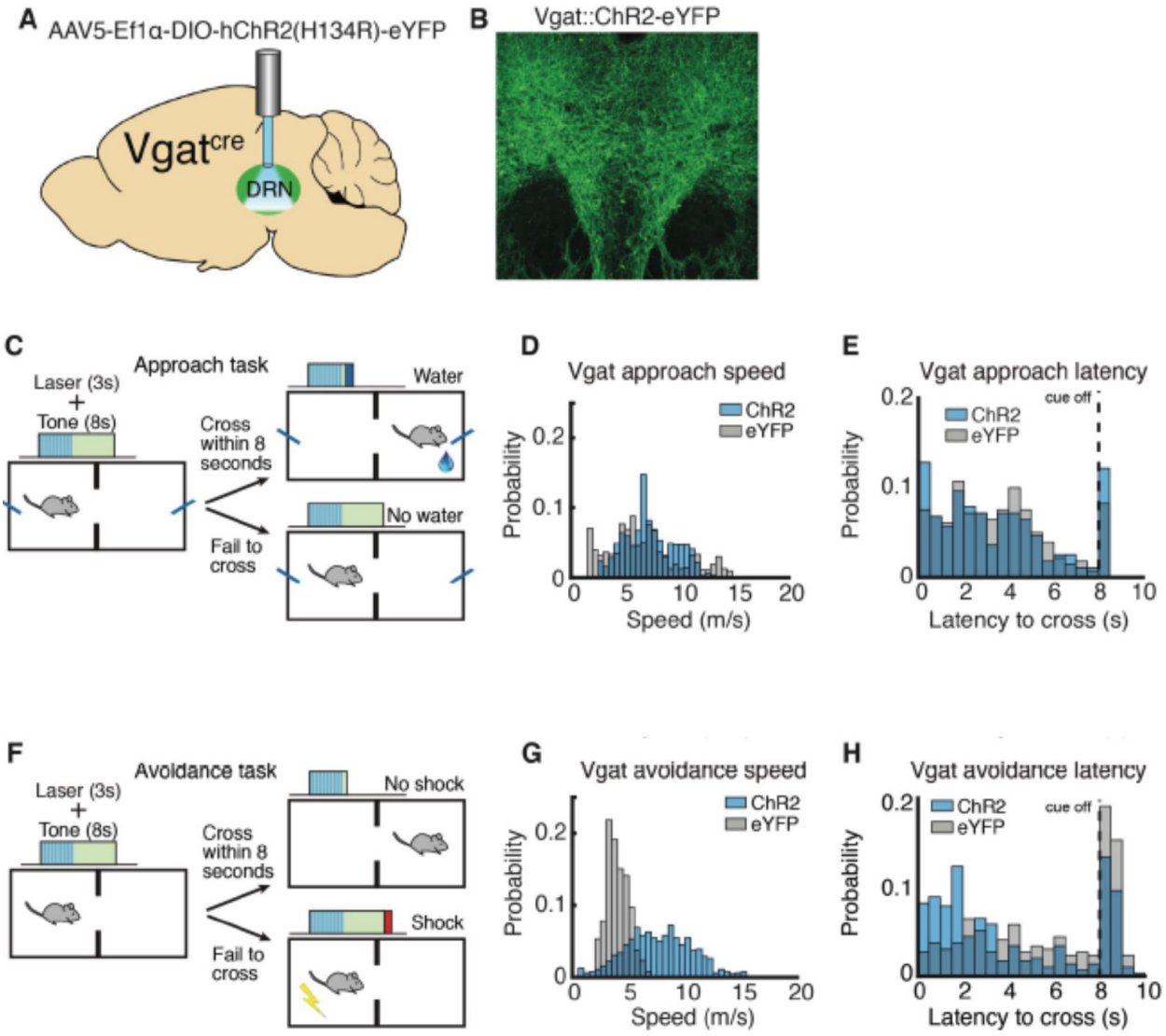

Fig. S12

(**A**) Dorsal raphe nucleus (DRN) viral vector and optical fiber placement schematic. (**B**) ChR2-eYFP expression in DRN GABA neurons in a Vgat-Cre mouse. (**C**) Optogenetic stimulation schematic in approach task. (**D**) Speed distribution during stimulation in approach task (Vgat::ChR2-eYFP, n=8; Vgat::eYFP, n=7). (**E**) Latency to cross after cue onset distribution, approach task. (Vgat::ChR2-eYFP, n=8; Vgat::eYFP, n=7; *P* = 0.62, log-rank test) (**F**) Optogenetic stimulation schematic in avoidance task. (**G**) Speed

distribution during stimulation in avoidance task (Vgat::ChR2-eYFP, n=8; Vgat::eYFP, n=7). (**H**) Latency to cross after cue onset distribution, avoidance task (Vgat::ChR2-eYFP, n=8; Vgat::eYFP, n=7; $P < 0.0001$, log-rank test).

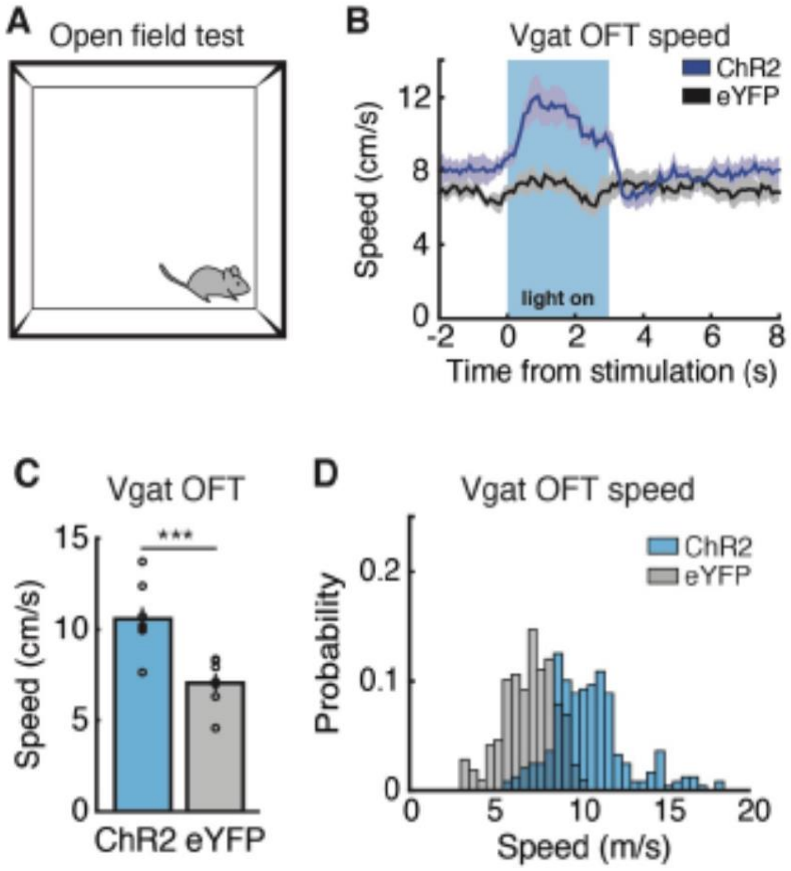

Fig. S13

(**A**) Open field test (OFT) schematic. (**B**) Speed aligned to stimulation onset, OFT (Vgat::ChR2-eYFP, n=8; Vgat::eYFP, n=7). (**C**) Mean speed during stimulation, OFT. (**D**) Speed distribution during stimulation in OFT. ***$P < 0.001$, Wilcoxon rank-sum test. Error bars indicate s.e.m.

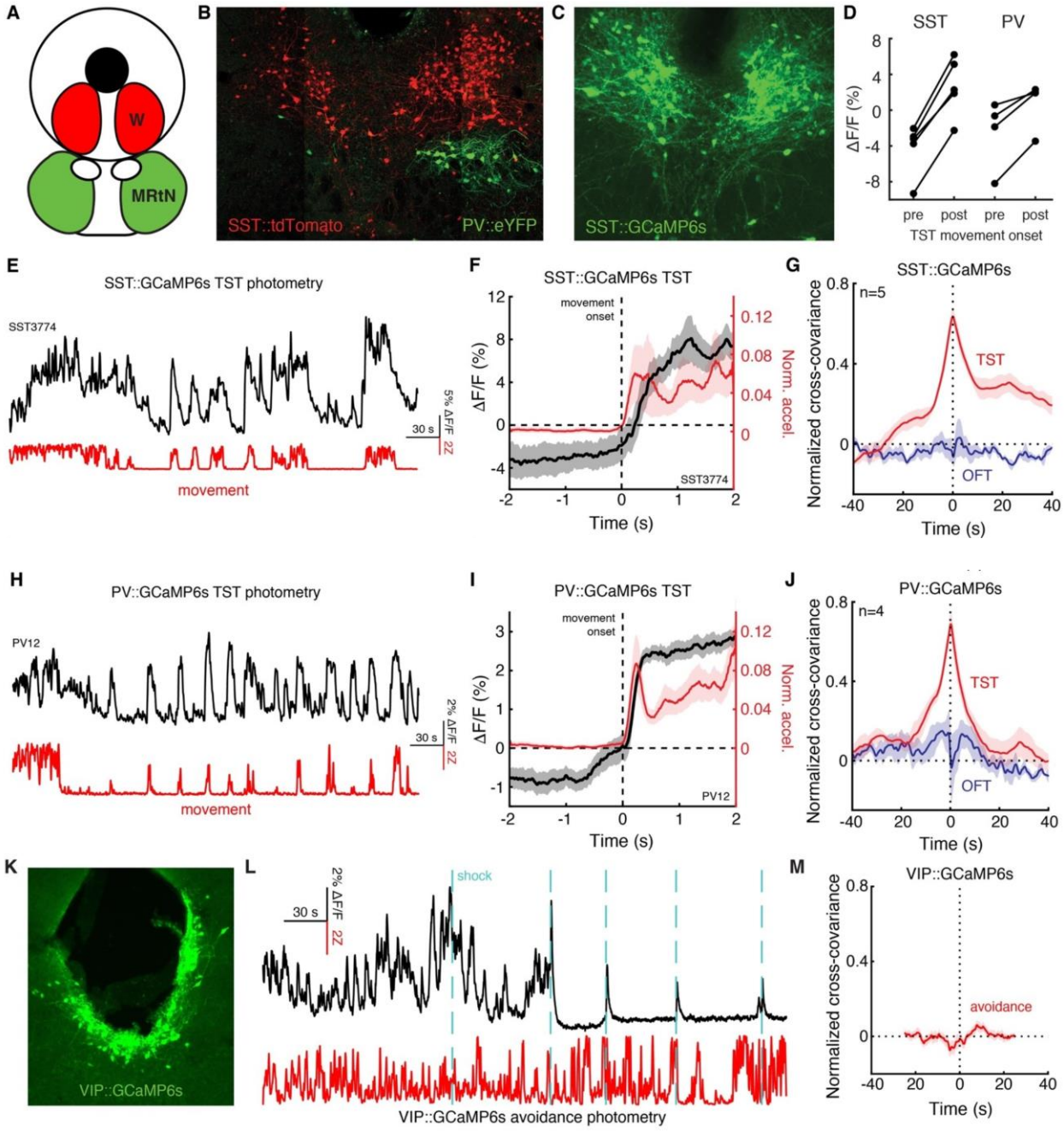

Fig. S14

(**A**) Schematic of regional DRN anatomy including DRN lateral wings (W) and adjacent midbrain reticular nucleus (MRtN). (**B**) tdTomato and eYFP expression in DRN somatostatin (SST) and MRtN parvalbumin (PV) neurons in a SST-Cre x PV-FlpO mouse.

(**C**) GCaMP6s expression in DRN SST neurons. (**D**) Mean ΔF/F before (pre) and after (post) TST movement onset in SST::GCaMP6s mice (n=5) and PV::GCaMP6s mice (n=4). (**E**) Example TST photometry data from a SST::GCaMP6s mouse. GCaMP ΔF/F in black, speed in red. (**F**) Mean ΔF/F aligned to TST movement onset for the mouse in panel E. (**G**) Mean normalized cross-covariance between movement and GCaMP6s ΔF/F in OFT and TST environments in SST mice (n=5). (**H**) Example TST photometry data from a PV::GCaMP6s mouse. GCaMP ΔF/F in black, speed in red. (**I**) Mean ΔF/F aligned to TST movement onset for the mouse in panel H. (**J**) Mean normalized cross-covariance between movement and GCaMP6s ΔF/F in OFT and TST environments in PV mice (n=4). (**K**) GCaMP6s expression in DRN VIP neurons in a VIP-Cre mouse. (**L**) Example avoidance photometry data from a VIP::GCaMP6s mouse. GCaMP ΔF/F in black, speed in red. (**M**) Normalized cross-covariance between movement and GCaMP6s ΔF/F during avoidance for the mouse in panel L. Error bars indicate s.e.m.

Chapter 4. Conclusions

Discussion

In the present work, I show that ‘fight-or-flight’ conditions invert the dynamics and functional role of DRN serotonin system: instead of saying ‘Stop’, in emergency situations 5-HT says ‘Go’. I used optical methods to monitor and control DRN serotonin neurons during movement in environments that ranged from rewarding to mildly aversive to escape-provoking. I found that when serotonin neurons were transiently stimulated in low – or medium- threat environments mice paused, but when the same serotonin population was stimulated in high-threat environments mice tried to escape. I then recorded from both DRN serotonin neurons at both population and single-cell level, and found that movement-related neural tuning ‘switched’ between environments – neural activity decreased when movement was initiated in low- or medium-threat environments but increased in high- threat environments. Additionally, I found that DRN GABA neurons also flip their dynamics and functional role, but this flip happens at a lower threat level – between environments with positive and negative valence.

There are several important points to consider in our experiments that may guide future approaches to understanding how the DRN system switches signals upon movement in different environmental contexts. In the following sections, I will discuss experimental caveats, speculate on possible scenarios for what is happening, and propose a revised model of serotonin function.

When does the 'switch' happen?

To examine DRN serotonin activity in different contexts, I used multiple behavioral environments, including the open field test (OFT), wheel running, tail suspension test (TST), reward approach, and punishment avoidance task in the operant chamber. Neural activity recording in the OFT, wheel running, and TST happened in one session to capture both 1) the transient movement signals and 2) the background signals that could reflect the environmental differences. The OFT is commonly used as a locomotor control test when assessing drug-induced physiological effects. It is also often used to test anxiety-like behavior by measuring the time spent in the center, because rodents generally try to avoid bright, open spaces (Felix-Ortiz et al., 2013). In contrast, wheel running is positively reinforcing for both laboratory and wild mice even without any external reward (Greenwood et al., 2011; Meijer and Robbers, 2014; Sherwin, 1998). The TST was first developed as a rodent screening test for potential human antidepressant drugs. Animals under the TST show immediate stressful escape responses, and repeated exposure to the TST can induce depression-like passive coping behavior.

With this evidence, I conclude that the environmental threat level may be a driving factor for the switch in DRN serotonin activity when regarding the OFT as a mid-threat environment, wheel running as a low-threat environment, and the TST as a high-threat environment. However, this interpretation may be oversimplified because of the qualitative differences in each environment. In addition, gross motor behavior differed in these three tasks, which may confound the interpretation of the data. To control for these

issues, we used the reward approach as well as and punishment avoidance tasks that require the same motor movement and placement in the same operant chamber, and result in opposite valence outcomes. However, in this study, I simply divided the task context as either positive (reward) or negative (shock), which only resulted in a qualitative difference in the valence. In the future, it would be informative to test how quantitative parameters of reward and shock tasks (e.g. duration, intensity, or proximity, etc.) contribute to the DRN neural activity switch. Lastly, each animal may "feel" the environmental valence differently, thus, measuring multiple features of animal behavior will provide latent information about how the ways the animal perceive the environment affect the DRN neural activity switch (Dolensek et al., 2020).

What is the source of the switch signal?

My data suggests that the switch signal observed in DRN serotonin and GABA neurons reflects an integration of the movement-related and environmental valence-related information. What is the source of these input signals? It is possible that transient movement signals come from the cortical motor areas, striatum, periaqueductal gray, or the cerebellum, which have been shown to be important for motor control and execution. The DRN also receives major inputs originating from the prefrontal cortex, hypothalamus, and amygdala that could potentially provide environmental valence information (Weissbourd, 2014). Although the anatomical inputs to the DRN are well mapped out, their functional roles in shaping DRN serotonin and GABA activity remains unknown. Another possibility is that the DRN receives movement signals that already reflect the environmental valence. A recent study found that separate populations of neurons in the

ventral pallidum (VP) opposingly encode the reward-seeking approach and punishment avoidance behaviors. The authors propose that the integration of the different VP populations may contribute to the switched signals in single neurons in the DRN (Stephenson-Jones et al., 2020). However, the VP does not send input directly to the DRN, but instead possibly via its connection to the habenula, and it is unclear in which form these signals reach the DRN.

Another candidate region is the habenula, which signals negative prediction error and sends direct input to the DRN (Bromberg-Martin and Hikosaka, 2011). A recent study shows that under a constant inescapable shock situation, the zebra fish changes its behavior from active escape to passive coping (reduced mobility). As the behavioral transition progresses over many minutes, habenular activity slowly increases while the raphe activity decreases (Andalman et al., 2019). This data also suggests that the habenula may encode the subjective perception of the environment and the change in behavioral strategy (since the context did not change), but only the *type* of coping method. Thus, it will be important to distinguish between the environmental valence set by the experimenter and the way the animal perceives the current environment through behavioral measures. For example, one could systematically change the environmental valence by changing reward size or shock level, and then measure how the animal behavior changes in each environment. The animal behavior can be explicitly expressed the way the animal responds to the stimuli (e.g. latency to get reward, reward consumption duration, or escape latency), or can be implicitly expressed (in pupil size, temperature, or overall movement). The idea that the DRN serotonin system may signal

the animal's behavioral strategy is also suggested in another recent study monitoring the whole brain activity while freely moving zebrafish larvae alternate between exploration and exploitation states during prey hunting (Marques et al., 2020). In this study, the DRN serotonin neural activity was persistently increased during the exploitation phase, and the habenular activity was transiently increased when the animal was transitioning from exploration to exploitation. In the exploitation state (where serotonin activity is generally higher), the animal generally moves less in a localized zone, but the hunting frequency increases, which still requires a sudden, explosive movement. Furthermore, this data suggests that behavior is hierarchically structured and cannot be simply described as increased or decreased movement. To test if serotonin activity tracks both fast- and slow-time scale activity, it would be interesting to examine how transient DRN serotonin activity changes during hunting bouts and test if the habenular trigger the DRN serotonin system to move to the adaptive state.

How is the switch signal shaped?

Our current knowledge about the DRN system does not place much constraint on what could be happening to shape the switch signals in different environments. It could be happening at a long-range input level, a local circuit level, or a dendritic level. An important finding from my work is that both DRN serotonin and GABA neural activity flip, but at a different thresholds. This was surprising, because I expected to see the opposing signal patterns from serotonin and GABA since multiple studies have shown that DRN GABA neurons inhibit DRN 5-HT neurons (Challis, 2013; Hernández-Vázquez et al., 2019). This view may be too simplistic, given recent evidence that GABA neurons in the

neuromodulator system may play an important role in shaping the activity of neuromodulators. For example, Cohen et al. found that VTA GABA neural activity was persistently increased in accordance with the reward size, suggesting that it signals reward expectation, an important variable for calculating reward prediction error signals seen in VTA dopamine neurons (Cohen et al., 2012). The same group later used optogenetic manipulation of VTA GABA neurons to show that these neurons casually contribute to prediction-error calculations in the VTA (Eshel et al., 2015). To understand the relationship between DRN serotonin and GABA neurons, future studies should systematically examine which environmental factors lead to the shifted threshold, and then examine the underlying circuit mechanism. Do DRN serotonin and GABA neural activity reside on the same spectrum (but shifted), or do they report distinct information content like VTA GABA neurons? First, one can test if in other contexts that can elicit 'flight or fight' behavior such as CO2 exposure, forced swim test, predator attacks, or extreme hunger state to test whether the switching activity is preserved. To control for movement differences, one can parametrize the valence of the environment (e.g. by modulating intensity, proximity, or duration, etc.) to examine if switching happens in the same environment.

To understand the possible local circuit mechanism, one can simultaneously record the serotonin population while also manipulating the local interneuron population to probe causal dependency. Preliminary recording in DRN GABA subtypes including PV, SST, and VIP neurons in a subset of behavioral testing offers some insight to the local mechanism. Both PV and SST neurons showed similar activity to DRN GABA neurons in

the TST, but without a functional manipulation experiment, it remains unknown how they communicate with the serotonin neurons. Interestingly, during the punishment avoidance task, VIP neuron activity was high and increased during first several shock deliveries, but significantly diminished thereafter. In many brain regions, VIP neurons inhibit PV and SOM neurons, resulting in disinhibitory effects on excitatory pyramidal neurons (Krabbe et al., 2019; Letzkus et al., 2011). While speculative, it is possible that VIP neurons shape DRN GABA neurons, since GABA activity during movement was coincidently switched after first few shocks. Finally, another possibility lies in the change in resting membrane potential in DRN neurons in different environments. Depending on the current membrane potential, the same input can have an excitatory or initiatory effect. Using recently developed voltage imaging or *in vivo* intracellular recording that are capable of observing subthreshold neural activity may provide insights into this hypothesis (Abdelfattah et al., 2019).

What is the relationship with other neuromodulatory systems?

The mammalian brain contains several neuromodulatory systems such as serotonin, dopamine, and norepinephrine. These systems typically modulate neural activity in multiple downstream regions via G-protein coupled receptors and influence a broad range of behaviors. How is the DRN connected to these systems? Dopamine neurons are found in the ventral tegemental area (VTA), and norepinephrine neurons are found in the locus coeruleus (LC), both located near the brainstem. The DRN serotonin system is interconnected with the VTA dopamine and the LC norepinephrine systems with reciprocal connections, and these neuromodulator systems express each other's

receptors. A recent study has found that while VTA dopamine neurons and DRN serotonin neurons are reciprocally connected, the DRN serotonin input to VTA dopamine neurons are about six times greater suggesting a hierarchical relationship between these two systems. (Ogawa et al., 2014). In addition to understanding the anatomical relationships between these systems, it would be essential to examine their functional roles in shaping each other's activity.

How do the other neuromodulatroy systems operate in the same or similar behavioral paradigms as I used? When rats were trained to perform lever press upon auditory cue presentation to prevent future shock, dopamine level in the nucleus accumbens (NAc) increased during cues that resulted in successful avoidance, but not during failed escaped trials (Oleson et al., 2012). These data suggest that dopamine signals compute positive value-coding in aversive contexts consistent with rewarding contexts. Another study has demonstrated a distinct functional contribution of projection-specific VTA dopamine neurons by showing that the lateral NAc projecting dopamine activity exhibit classical reward-predictive signals while medial NAc projecting dopamine activity is excited by unexpected aversive outcomes only (de Jong et al., 2019). While these data suggest an important role of the dopamine system in reward approach and punishment avoidance behavior, unfortunately, a direct comparison with my dissertation data is difficult because these researchers have only looked at passive neural response to the experimental cues and outcomes, but not during action phases.

Like the other neuromodulators, the LC norepinephrine system has a widespread network in the brain and modulates sleep, arousal, and learning (Aston-Jones and Cohen, 2005). Its activity precedes pupil dilation, which is used as a measure of arousal state (Larsen and Waters, 2018). Interestingly, constant tonic (3Hz) activation of the LC norepinephrine system promotes behavioral arousal, but phasic (5Hz or greater) activation results in behavioral arrest (Carter et al., 2010). However, as Carter et al. note, without monitoring endogenous activity of LC norepinephrine neurons in the same context, it remains unclear whether this behavioral effect was a consequence of artificial regulation. Nevertheless, this finding suggests a possible bidirectional role of the LC norepinephrine system in modulating behavioral state, which is reminiscent to my finding.

What is the computational role of the switch signal?

My data demonstrates that DRN serotonin and GABA neural activity not only correlate with movement, but that they can casually drive environment-dependent movement. In line with the finding that the activation of DRN serotonin inhibits movement in low- or mid-threat environments, there seems to be an evolutionarily preserved role of serotonin in behavioral inhibition across evolutionary taxa as seen other works using *C. elegans*, drosophila, zebra fish, and mice (Correia et al., 2017; Flavell et al., 2013; Howard et al., 2019; Kawashima et al., 2016). Despite the differences in the experimental set-ups and interpretations, Soubrié's 'behavioral inhibition' theory of serotonin seems to hold somewhat true. Although this theory has been supported in many indirect studies, only a recent development in spatiotemporally defined manipulation and recording of serotonin neurons has allowed researchers to confirm the hypothesis. However, a gap remains

between acknowledging the behavioral phenotype of serotonin activation and determining what serotonin could be functionally relevant to. For example, long before finding prediction error-like signals in VTA dopamine neurons, it was well known that drugs that release dopamine increase locomotor activity. What are the possible computational roles of serotonin associated with behavioral inhibition?

One computational theory suggests that behavioral inhibition serves to promote active waiting for delayed reward, which is expressed as a discounting factor in reinforcement learning theory (Doya, 2008). Indeed, multiple recent findings have shown that DRN serotonin neurons are more active during active waiting, and activation of DRN serotonin neurons increases the waiting period (Fonseca et al., 2015; Miyazaki et al., 2011, 2012, 2014). While this theory is well supported in the tested experimental contexts, some findings with different experimental questions and settings still cannot readily be integrated. For example, serotonin release slowly increases when animals receive inescapable shocks, but not during escapable shocks (Amat et al., 1998, 2005). In my data, DRN serotonin activity increased during failed avoidance trials and during movement epochs in the TST. These data indicate that serotonin activity can increase during non-waiting periods or active movement. How can these seemingly opposing results be reconciled?

Here, I propose a revised model in which the DRN serotonin system switches sensorimotor attention to promote adaptive behavior most suited to the current environment. In the OFT using fiber photometry, I found that DRN serotonin activity

sharply decreases when an animal is initiating a movement. However, single-cell recording using microendoscopy revealed that different subsets of individual serotonin neurons are persistently active during non-movement epochs and quiet during movement epochs. It is likely that fiber photometry, which records the bulk average fluorescence activity, was not able to distinguish this difference because the baseline activity is formed by the average activity of many neurons. This informs us that there is a non-uniform excitatory mechanism that heterogeneously increases serotonin activity. It remains unknown whether the heterogeneity arises from one or multiple input sources, but it is possible that the DRN integrates diverse sensorimotor and environmental information. In addition, it would be essential to test if the heterogeneity is associated with the outputs of the DRN. Multiple studies have already shown that DRN serotonin neurons exhibit heterogeneous activity in reward- and punishment- learning tasks (Cohen et al., 2015b; Hayashi et al., 2015). A more recent study has demonstrated that cortical-projecting DRN serotonin neurons are inhibited by punishment, but subcortical-projecting neurons are activated by punishment (Ren et al., 2018). In a subsequent study, the same group used single-cell RNA sequencing to show that these two groups of DRN serotonin neurons express unique molecular markers, further strengthening the idea of projection specific functional role of the DRN serotonin system (Ren et al., 2019).

I speculate that a different ensemble of serotonin neurons can result in functionally distinct ‘behavioral inhibition’-like phenotypes via specific anatomical connections throughout the brain. Animals exhibit intermittent locomotion where they adjust behavior to perform active sensation or movement in changing circumstances (Kramer and

McLaughlin, 2001). Most studies have only focused on measuring the gross locomotor state with increased serotonin; however, I speculate that serotonin release also promotes fine muscle movements such as whisker, nose, and ocular movements which accompany specific active sensation with gross motor inhibition. In order to study this, it will be essential to adopt new machine learning techniques used for measuring and identifying fine behavior structures (Mathis and Mathis, 2019; Wiltschko et al., 2015).

Serotonin can facilitate movement when the current circumstance requires switching from active sensation to active motion. Microendoscopy recording revealed that most DRN serotonin neurons were uniformly activated during each movement epoch in the TST with less heterogeneity. This indicates that in an escape situation where both active sensation and movement is required, DRN serotonin may send a global behavioral switching signal to prioritize the most adaptive behavior. Escape behaviors, once thought to be non-cognitive and reflexive, turn out to require decision-making and action selection processes that must be flexible in each environment (Branco and Redgrave, 2020). I speculate that serotonin shifts sensorimotor attention by modulating downstream brain areas in order to promote adaptive behaviors such as threat detection and escape initiation.

Examining DRN serotonin and GABA function through the clarifying lens of movement revealed that this major neuromodulatory system operates in two distinct modes – a movement-facilitating mode in fight-or-flight conditions, and a movement-suppressing mode in all other studied environments. These results have major

implications for theoretical models of serotonin function and for understanding the impact of serotonin-targeted therapeutic interventions on brain function in normal and disease states. We show that serotonin dynamics and function flip in the tail suspension test, widely used as an antidepressant drug screen; accounting for state-dependent function may accelerate the development of new serotonin-targeted therapies. More generally, considering the widespread distribution of dorsal raphe serotonin axons throughout the cortex and striatum, this finding raises the possibility that the 'emergency brain' operates in a fundamentally different way than previously thought; the functional flip of this widely-distributed system in emergency situations suggests that this phenomenon is not isolated, but may instead reflect a general principle of brain function.

Materials and Methods

All procedures conformed to guidelines established by the National Institutes of Health and have been approved by the Cornell University Institutional Animal Care and Use Committee.

Subjects

SERT-Cre (Ross McDevitt, NIH/NIDA & Xiaoxi Zhuang, University of Chicago) and Vgat-Cre, SST-Cre, PV-Cre, and VIP-Cre (The Jackson Laboratory, Bar Harbor, ME) mice (postnatal 3-6 months) were used for 5-HT- and GABA-specific viral vector expression. All Cre driver lines were fully backcrossed to C57BL/6J mice. All mice were male and housed in groups, and were maintained on a 12-hour reverse light-dark cycle with *ad libitum* access to food and water, except during approach conditioning.

Viral vectors

For photometry and microendoscopy experiments, we used AAV5-CAG-FLEX-GCaMP6s (Penn Vector Core, Philadelphia, PA), AAVdj-Ef1α-DIO-GCaMP6m (Stanford Vector Core, Stanford, CA), or AAV5-CAG-FLEX-GFP (UNC Vector Core, Chapel Hill, NC). For optogenetic experiments, we used AAV5-Ef1α-DIO-hChR2(H134R)-eYFP or AAV5-Ef1α-DIO-eYFP (UNC Vector Core, Chapel Hill, NC).

Surgery

Mice were deeply anesthetized with isoflurane (5%). Fur was trimmed, and mice were placed in a stereotaxic frame (Kopf Instruments, Tujunga, CA). A heating pad was

used to prevent hypothermia. Isoflurane was delivered at 1-3% throughout surgery; this level was adjusted to maintain a constant surgical plane. Ophthalmic ointment was used to protect the eyes. Buprenorphine (0.05 mg/kg, subcutaneous) was given before the start of surgery. A mixture of 0.5% lidocaine and 0.25% bupivacaine (100 µL) was injected subdermally along the incision line. The scalp was disinfected with betadine and alcohol. A midline incision exposed the skull, which was thoroughly cleaned, and a craniotomy was made above the DRN. Virus was targeted to the DRN (-4.5 AP, 0.0 ML, -3.3 & -3.0 DV), and slowly pressure injected (100 nl/min) using a 10 µL Hamilton syringe (nanofil; WPI, Sarasota, FL), a 33 gauge beveled needle, and a micro-syringe pump controller (Micro 4; WPI, Sarasota, FL). After each injection the needle was left in place for 10 minutes and then slowly withdrawn.

For photometry and microendoscopy experiments, a total of 700 nl (350 nl at each DV site) of vector was injected. For optogenetic experiments, a total of 800 nl (400 nl at each DV site) of vector was used. For photometry and optogenetic experiments an optical fiber embedded in a metal ferrule was implanted at 15° (-4.5 AP, 0.5 ML, -2.8 DV). A 400 µm diameter, 0.48 NA optical fiber (Doric Lenses, Québec, Canada) was used for photometry experiments, and a 200 µm diameter, 0.22 NA optical fiber (Thorlabs Inc., Newton, NJ) was used for optogenetic experiments. For microendoscopy experiments, animals were implanted with a 6 mm long, 500 µm diameter GRIN lens (Inscopix, Palo Alto, CA) at 15° (-4.5 AP, 1.1 ML, -3.3 DV). A layer of metabond (Parkell, Inc., Edgewood, NY) and dental acrylic (Lang Dental Manufacturing, Wheeling, IL) was applied to firmly hold the implant in place, and the surrounding skin was sutured closed. Post-operative

buprenorphine (0.05 mg/kg), carprofen (5 mg/kg), and lactated ringers (500 µL) were administered subcutaneously. For microendoscopy, a baseplate was implanted above the GRIN lens after 3 weeks. Virus was allowed to express for a minimum of 3 weeks before behavioral testing.

Fiber photometry

Fiber photometry was performed as previously described. 473 nm and 405 nm data were collected for all GCaMP and GFP photometry experiments. 473 nm and 405 nm diode lasers (Omicron Luxx, Rodgau-Dudenhofen, Germany) were modulated at 700 Hz and 500 Hz, respectively, using a dual optical chopper (New Focus Model 3502, Newport, Irvine, CA). Both laser beams were combined using a mirror (KM100-E02, Thorlabs, Newton, NJ) and a dichroic filter (LM01-427, Semrock, Rochester, NY), and the power was adjusted using a neutral density filter to 15-100 µW. Power-adjusted laser beans were aligned to a fluorescence filter cube (DFMB, Thorlabs, Newton, NJ), where the excitation beams were reflected with a dichroic filter (FF495, Semrock, Rochester, NY), collimated (F240FC-A with AD11F, Thorlabs, Newton, NJ), and coupled to an optical patch cord (400 µm, Doric Lenses, Quebec, Canada). Emitted fluorescence was passed through a dichroic filter (FF495, Semrock, Rochester, NY) and a bandpass filter (FF03-525/50, Semrock, Rochester, NY), and was collected by a femtowatt photoreceiver (New Focus 2151, Newport, Irvine, CA). Outputs from the photoreceiver were directed through two lock-in amplifiers (SR810 DSP, Stanford Research System, Sunnyvale, CA), digitized using a DAQ (U6 pro, LabJack, Lakewood, CL) at a sampling rate of 250 Hz, and recorded by custom-modified LabJack software.

Optogenetic stimulation

During behavioral testing an external optical fiber (200 μm diameter, 0.22 NA, Doric Lenses, Québec, Canada) was coupled to the implanted fiber optic with a zirconia sleeve. An optical commutator allowed for unrestricted rotation (Doric Lenses, Québec, Canada). Optical stimulation was provided with a 100 mW 473 nm diode pumped solid state laser (OEM Laser Systems, Inc., Salt Lake City, UT) and controlled by a Master-8 stimulus generator (A.M.P.I., Jerusalem, Israel). Trains of 25 Hz, 10 ms light pulses were used for all ChR2 experiments. Stimulation experiments used 6 mW light (47.73 mW/mm^2 at the fiber tip), with stimulation epoch length dependent on the behavioral task.

Microendoscopy

Prior to behavioral testing animals were briefly anaesthetized to attach the microendoscope to the baseplate (Inscopix, Palo Alto, CA). Imaging data was acquired at 20 Hz for 15 minutes in the OFT and 15 minutes in the TST. Fluorescence videos were preprocessed, down-sampled to 10 Hz, spatially filtered, and motion corrected using Inscopix software. Videos were exported and processed with MIN1PIPE (Lu et al., 2018), where background was subtracted, motion was corrected, and neural signal was extracted. MIN1PIPE seeds were picked manually, and code was modified to remove the > 0 constraint on temporal components. Data was processed separately for the OFT and the TST.

Behavioral testing: open field test (OFT), tail suspension test (TST), and wheel

Mouse behavior was recorded at 30 fps with a USB 3.0 camera (Chameleon3, Pointgrey, Richmond, BC, Canada) during all behavioral testing sessions. A Labjack DAQ (U6 pro, LabJack, Lakewood, CL) was used to acquire all behavioral data. The sequence of behavioral tests follows the individual test descriptions.

OFT (photometry): A 50 x 50 cm arena made of white Plexiglas was divided into large (50 x 42 x 37.5 x 32 cm, used for open field testing) and small (used for wheel testing) subsections. Testing took place under bright room light. Mice were placed in the center of the large arena at the start of each OFT and allowed to freely explore for 6 minutes. Movement was tracked using Ethovision (Noldus, Leesburg, VA).

Wheel (photometry): 4-6 weeks after surgery, a running wheel (Ware Manufacturing, Amazon) was introduced to the home cage for about a week for acclimation. During testing, the running wheel was placed into the small subsection of the OFT, described above. Animals were placed into this section and allowed to freely engage in running behavior on the wheel for 20 minutes. Wheel movement was captured by an optical encoder (E4T 200 cycles per revolution, US Digital, Vancouver, WA) attached to the bottom part of the wheel shaft.

TST (photometry): The mouse's tail was taped to a 40 cm high horizontal bar, and the mouse was suspended by its tail for 6 minutes. Struggling behavior was recorded using an accelerometer taped to the tail.

Testing sequence (photometry): On photometry recording days, mice were plugged into an optical patch cord connected to the fiber photometry data acquisition rig and were exposed to the following series of behavioral experiments: OFT – Wheel – OFT – TST – OFT. Mice were moved by the experimenter between each behavioral test without disconnection from the fiber photometry system so that data could be continuously recorded. Conditions and timing for each test were as described above. While the animal was in the second OFT, wheel running data were analyzed. If mice performed multiple bouts of wheel running with a duration greater than five seconds on the wheel, mice were moved from the OFT to the TST, and then back to the last OFT. If running behavior did not meet this criteria, mice were brought back to the home cage and tested on subsequent days; if criteria were never met, mice were excluded from further study.

OFT (optogenetics): A 50 × 50 cm arena made of white Plexiglas was used as an open field under bright room light. Mice were placed in the center of the arena at the start of each session. The stimulation protocol used for this open-field test replicated the phasic optogenetic stimulation protocol outlined by Correia et al. (2017). The protocol consisted of 5-minute blocks alternating between stimulation and no-stimulation. During stimulation blocks, light was delivered for 3 seconds followed by a 7-second pause, a pattern that repeated throughout the block. The session began with a no-stimulation block for a total session time of 30 minutes (OFF-ON-OFF-ON-OFF-ON).

Wheel (optogenetics): A running wheel was introduced to the home cage for acclimation. About a week later, mice were acclimated to the running wheel in the OFT

arena, surrounded by temporary walls to provide an enclosed space. On a control day, mice were tethered to a patch cord and allowed to freely run on the wheel for 20 minutes. On a following experimental day, the session began with a 5-minute no-stimulation block followed by 3-minute blocks alternating between stimulation and no-stimulation for a total session time of 20 minutes (OFF-ON-OFF-ON-OFF-ON). For Vgat::ChR2 groups, 25 Hz 10 ms light pulses were continuously delivered during the stimulation block.

TST (optogenetics): Mice were tethered to a patch cord and the tail was taped to an accelerometer attached to a horizontal bar 40 cm from the ground. The protocol consisted of 3-minute blocks alternating between stimulation and no-stimulation blocks. The session began with a no-stimulation block for a total session time of 18 minutes (OFF-ON-OFF-ON-OFF-ON). For SERT::ChR2 groups, 25 Hz 10 ms light pulses were delivered for 3 seconds followed by a 7-second pause, a pattern that repeated throughout the block. For Vgat::ChR2 groups, 25 Hz 10 ms light pulses were continuously delivered during the stimulation block.

Behavioral testing: reward approach and shock avoidance tasks

Reward approach and shock avoidance tasks were performed in metal rectangular shuttle boxes divided into two equal compartments by Plexiglas semi-partitions, which allowed animals to move freely between compartments. A 17.25” W x 6.75” D x 10” H shuttle box (MedAssociates, Fairfax, VT) was used for SERT::GCaMP, SERT::ChR2, and Vgat::ChR2 experiments, and a 14” W x 7” D x 12” H shuttle box (Coulbourn Instruments, Whitehall, PA) was used for Vgat::GCaMP experiments. All shuttle box experiments were

done in the dark. Mice were tracked using infrared detectors located alongside the chambers and an infrared USB 3.0 camera (Chameleon3, Pointgrey, Richmond, BC, Canada). All signals from the shuttle boxes were converted to TTL (SuperPort 16 Output Module, MedAssociates, Fairfax, VT or Habitest Linc Output Converter, Coulbourn Instruments, Whitehall, PA) and collected by the Labjack DAQ (U6 pro, LabJack, Lakewood, CL). For approach experiments, walls at the end of each compartment were equipped with lick spouts for water delivery and lick detection.

Approach conditioning: Mice were water restricted prior to approach conditioning. Body mass was measured daily to maintain at least 80% baseline body weight. For training, a tone (4 kHz or 12 kHz at 60 dB, counterbalanced between approach and avoidance tasks) was played indefinitely until mice crossed the chamber. When crossed, 20 µl of water was delivered to the lick spout in the goal chamber. Tones occurred pseudo-randomly with an average inter-trial interval (ITI) of 40 seconds after water consumption, and mice were given the opportunity to perform 30-50 trials per day. After several days of training, mice were switched to a testing protocol, which used a tone with a maximum 8-second duration. Mice were required to cross the chamber within this 8-second window for successful water delivery. If mice crossed the chamber within 8 seconds, the tone was terminated and water was delivered to the goal compartment. However, if mice did not cross the chamber within 8 seconds, the tone was terminated at 8 seconds and no water was delivered.

Approach (optogenetics): After learning criteria were met, on the control day mice were tethered to a patch cord and performed the behavioral task with no light delivery. On a following experimental day, stimulation light was delivered on every trial, starting at tone onset. Light was always delivered for 3 seconds, regardless of behavioral outcome.

Avoidance conditioning: A tone (4 kHz or 12 kHz, 60 dB, counterbalanced between approach and avoidance tasks) was played for 8 seconds pseudo-randomly with an average ITI of 40 seconds. If mice did not cross the chamber within 8 seconds, electric footshock (0.2 mA - 0.4 mA) was delivered through the grid floor until mice crossed the chamber (escape, or failed avoidance trials). If mice crossed within 8 seconds, the tone terminated and there was no shock (avoidance trials). Animals performed 30-40 trials per day.

Avoidance (optogenetics): After learning criteria were met, on the control day mice were tethered to a patch cord and performed the behavioral task with no light delivery. On a following experimental day, stimulation light was delivered on every trial, starting at tone onset. Light was always delivered for 3 seconds, regardless of behavioral outcome.

Perfusion and histological verification

Following experiments, animals were deeply anesthetized with Fatal-Plus at a dose of 90 mg/kg and transcardially perfused with 20 ml of PBS (phosphate-buffered saline), followed by 20 ml of 4% paraformaldehyde solution. Brains were extracted and stored overnight at 4°C in 4% paraformaldehyde solution. After 24 hours, brains were transferred

to 30% sucrose solution and allowed to equilibrate for at least 3 days. Brains were sectioned coronally (40 μm) on a freezing microtome. Sections were washed in PBS and mounted on slides with PVA-DABCO. Images were acquired using a Zeiss LSM 800 confocal scanning laser microscope with a 20X air objective.

Data analysis

All data analysis and statistical tests were performed using custom-written scripts in MATLAB (MathWorks, Natick, MA) and GraphPad Prism (GraphPad Software, San Diego, CA).

Statistics: Tabulated statistical results are presented in Table S1. Error bars and shaded areas report standard error of the mean (s.e.m.). All statistical tests were two-tailed. Within-subject analyses were performed using the Wilcoxon signed-rank test, and between-subject analyses were performed using the Wilcoxon rank-sum test. All latency comparisons were performed using the Mantel-Cox log-rank test to account for the fact that failed trials in the approach task had unknown true latencies (since, by definition, latencies in these trials were greater than the 8-second cut-off time). This test was developed for population survival analyses, and is appropriate and unbiased for right-censored data of this form. Cross-covariogram confidence intervals were computed using a circular block bootstrap with random block length (Politis and Romano, 1994).

Fiber photometry: Raw 473 nm and 405 nm channels were low-pass filtered at 20 Hz. The 405 nm reference channel was fit to the 473 nm channel using linear least

squares. Relative fluorescence changes, reported as ΔF/F, were calculated using the following equation:

$$\frac{\Delta F}{F_0} = \frac{\text{473 nm signal-fitted 405 nm signal}}{\text{mean 473 nm signal}} \times 100$$

Open Field Test: Movement onsets were defined by at least 2 seconds of < 2 cm/s speed followed by at least 2 seconds of > 2 cm/s speed. Group photometry analyses compared mean ΔF/F 1.5 seconds before and after movement onset. Optogenetic analyses compared ChR2 and eYFP mean speed during the 3-second stimulation period.

Approach task: Speed was thresholded at 3 cm/s to find movement onsets and offsets. Movements to cross the chamber were identified as the last movement onset during the tone. Data analysis only included trials with less than 3 seconds between chamber crossing and the first lick. Movement offsets were defined as < 3 cm/s speed following movement of at least 1 second of < 3 cm/s speed. Group photometry analyses compared mean ΔF/F 1.5 seconds before and after movement onset/offset. Optogenetic speed analyses compared ChR2 and eYFP mean speed during the 3-second stimulation period. Optogenetic latency analyses compared ChR2 and eYFP latency distributions using the log-rank test, discussed above. For these, all failed trials (where the mouse did not cross the chamber within 8 seconds) are grouped together and plotted at the 8-second point, since there is no latency information by definition for these trials. The log-rank statistical test (discussed above) accounts for this feature of latency datasets.

Avoidance task: Speed was thresholded at 1 cm/s to find movement onsets. Trials were divided into avoidance and failed avoidance (escape) trials with latencies respectively smaller or greater than the maximum tone duration (8 seconds). For avoidance trials, movements to cross the chamber were identified as the last movement onset during the tone. For failed avoidance data analysis, we used data from the first avoidance session. Shock-induced movement onsets were identified as the first movement onset during the shock. Movement offsets were defined as < 1 cm/s speed following movement of at least 1 second at > 5 cm/s speed. Group photometry data analysis compared mean ΔF/F 1.5 seconds before and after movement onset. For analyzing within-day response changes, the first avoidance day data was divided into 10 bins (1 pre-shock and 9 post-shock bins). Movement onsets that occurred between shocks (starting 5 seconds after shock and ending 8 seconds before shock) were included in the analysis. For each bin, the group photometry data compared the difference of mean □F/F 1.5 seconds before and after movement onset was calculated. Optogenetic speed analyses compared ChR2 and eYFP mean speed during the 3-second stimulation period. Optogenetic latency analyses compared ChR2 and eYFP latency distributions using the log-rank test, discussed above. Although we have complete latency information for avoidance trials, since the moment when the shock was escaped was recorded, we analyzed these data with methods identical to those used for the approach task (the log-rank statistical test) to ensure an equally-powered comparison.

Tail Suspension Test (TST): Data following 2 minutes of TST exposure was used for both photometry and optogenetic data analysis. Movement onset/offset calculation: The

z-score of the raw accelerometer data was calculated, and data were rectified, thresholded above 0.3-0.6, and binned into 100 ms bins, so that the value of each bin reflected the fraction of samples above threshold. Movement onset was defined as bin transition from zero to non-zero, with a pre-onset requirement of < 0.02 for at least 2 seconds and a post-onset requirement of >0.06 for at least 2 seconds. If onsets were within 0.8 seconds of each other they were combined. Final movement bouts were required to be at least 2 seconds long. Movement offset was defined as bin transition from non-zero to zero. Movement calculation for display only: Raw accelerometer data were rectified and normalized to the maximum value. Data for each movement onset (as defined above) was averaged and smoothed with a 50-sample moving average. Population photometry data compared mean ΔF/F during 1.5 seconds before and after movement onset. For optogenetic SERT groups, the epochs immediately before (-2 seconds to 0 seconds) and after (0 seconds to 3 seconds) light onset were analyzed. The difference in movement between these two epochs was compared between ChR2-eYFP and eYFP groups. For optogenetic Vgat groups, the time spent mobile during light stimulation was compared between ChR2-eYFP and eYFP groups.

Wheel. Data following 2 minutes of wheel exposure were used for both photometry and optogenetic data analysis. Running rate was calculated as the number of raw optical encoder samples per 100 ms bin. Movement onsets were calculated by normalizing running rate to the maximum for each animal, and then extracting all epochs that met the following criteria: at least 2 seconds of < 0.1 movement followed by at least 5 seconds of > 0.1 movement. Speed was determined using sampling rate and wheel diameter, and

was low pass filtered at 5 Hz for display purposes only. Population photometry data compared mean ΔF/F 2 seconds before and 5 seconds after movement onset. For optogenetic Vgat groups the time spent mobile during light stimulation was compared between ChR2-eYFP and eYFP groups.

Acknowledgments: We thank T.J. Davidson and C.B. Schaffer for photometry advice; T. Bollu for technical advice; P. Dayan, I.T. Ellwood, R.M. Harris-Warrick, R.R. Hoy, J.H. Goldberg, J.R. Fetcho, E. Troconis, D.A. Bulkin, and B. Sleezer for helpful discussions and/or comments on the manuscript; U. Lee for contributions to figure design; A.K. Recknagel for expert technical assistance; and the Warden laboratory and Cornell Neurobiology and Behavior for training and support. **Funding:** Supported by the Mong Family Foundation (C.S., Y.Y.H., A.G.), the Taiwan Ministry of Education (Y.Y.H), NIH DP2MH109982 (M.R.W), the Alfred P. Sloan Foundation (M.R.W.), the Whitehall Foundation (M.R.W.), and the Brain and Behavior Research Foundation (M.R.W). M.R.W. is a Robertson Neuroscience Investigator–New York Stem Cell Foundation. **Author contributions:** C.S. and M.R.W. conceived the project and designed the experiments; C.S., M.J., C.B., and N.K. performed stereotaxic surgery and histology; C.S., M.J., C.B., N.K., and D.K. conducted photometry and optogenetic experiments; C.S. and Y.Y.H. developed the behavioral data acquisition methods; C.S., M.J., A.G., E.W., C.S., and M.R.W. analyzed the data; C.S. and M.R.W. prepared the manuscript; M.R.W. supervised all aspects of the work. **Competing interests:** The authors declare no competing financial interests. **Data and materials availability:** All data are available in the manuscript or the supplementary materials.

References

Abdelfattah, A.S., Kawashima, T., Singh, A., Novak, O., Liu, H., Shuai, Y., Huang, Y.-C., Campagnola, L., Seeman, S.C., Yu, J., et al. (2019). Bright and photostable chemigenetic indicators for extended in vivo voltage imaging. Science *365*, 699–704.

Amat, J., Matus-Amat, P., Watkins, L.R., and Maier, S.F. (1998). Escapable and inescapable stress differentially alter extracellular levels of 5-HT in the basolateral amygdala of the rat. Brain Research *812*, 113–120.

Amat, J., Baratta, M.V., Paul, E., Bland, S.T., Watkins, L.R., and Maier, S.F. (2005). Medial prefrontal cortex determines how stressor controllability affects behavior and dorsal raphe nucleus. Nature Neuroscience *8*, 365–371.

Aston-Jones, G., and Cohen, J.D. (2005). AN INTEGRATIVE THEORY OF LOCUS COERULEUS-NOREPINEPHRINE FUNCTION: Adaptive Gain and Optimal Performance. Annual Review of Neuroscience *28*, 403–450.

Berridge, K.C. (2004). Motivation concepts in behavioral neuroscience. Physiology & Behavior *81*, 179–209.

Bonanni, L., Thomas, A., and Onofrj, M. (2010). Paradoxical kinesia in parkinsonian patients surviving earthquake. Movement Disorders *25*, 1302–1304.

Boyden, E.S., Zhang, F., Bamberg, E., Nagel, G., and Deisseroth, K. (2005). Millisecond-timescale, genetically targeted optical control of neural activity. Nature Neurosci. *8*, 1263–1268.

Branco, T., and Redgrave, P. (2020). The Neural Basis of Escape Behavior in Vertebrates. Annu. Rev. Neurosci. *43*, annurev-neuro-100219-122527.

Bruchas, M.R., Land, B.B., Aita, M., Xu, M., Barot, S.K., Li, S., and Chavkin, C. (2007). Stress-induced p38 mitogen-activated protein kinase activation mediates kappa-opioid-dependent dysphoria. J. Neurosci. *27*, 11614–11623.

Carhart-Harris, R.L., Bolstridge, M., Rucker, J., Day, C.M.J., Erritzoe, D., Kaelen, M., Bloomfield, M., Rickard, J.A., Forbes, B., Feilding, A., et al. (2016). Psilocybin with psychological support for treatment-resistant depression: an open-label feasibility study. The Lancet Psychiatry *3*, 619–627.

Carter, M.E., Yizhar, O., Chikahisa, S., Nguyen, H., Adamantidis, A., Nishino, S., Deisseroth, K., and de Lecea, L. (2010). Tuning arousal with optogenetic modulation of locus coeruleus neurons. Nat Neurosci *13*, 1526–1533.

Celada, P., Puig, M. V, Casanovas, J.M., Guillazo, G., and Artigas, F. (2001). Control of dorsal raphe serotonergic neurons by the medial prefrontal cortex: Involvement of serotonin-1A, GABA(A), and glutamate receptors. J. Neurosci. *21*, 9917–9929.

Challis, C. (2013). Raphe GABAergic neurons mediate the acquisition of avoidance after social defeat. J. Neurosci *33*, 13978–88, 13988.

Challis, C., Boulden, J., Veerakumar, A., Espallergues, J., Vassoler, F.M., Pierce, R.C., Beck, S.G., and Berton, O. (2013). Raphe GABAergic neurons mediate the acquisition of avoidance after social defeat. The Journal of Neuroscience *33*, 13978–13988, 13988a.

Chen, T.-W., Wardill, T.J., Sun, Y., Pulver, S.R., Renninger, S.L., Baohan, A., Schreiter, E.R., Kerr, R. a., Orger, M.B., Jayaraman, V., et al. (2013). Ultrasensitive fluorescent proteins for imaging neuronal activity. Nature *499*, 295–300.

Cohen, J.Y., Haesler, S., Vong, L., Lowell, B.B., and Uchida, N. (2012). Neuron-type specific signals for reward and punishment in the ventral tegmental area. Nature *482*, 85–88.

Cohen, J.Y., Amoroso, M.W., and Uchida, N. (2015a). Serotonergic neurons signal reward and punishment on multiple timescales. ELIFE 06346.

Cohen, J.Y., Amoroso, M.W., and Uchida, N. (2015b). Serotonergic neurons signal reward and punishment on multiple timescales. Elife *6346*.

Commons, K.G., Cholanians, A.B., Babb, J.A., and Ehlinger, D.G. (2017). The Rodent Forced Swim Test Measures Stress-Coping Strategy, Not Depression-like Behavior. ACS Chemical Neuroscience *8*, 955–960.

Correia, P.A., Lottem, E., Banerjee, D., Machado, A.S., Carey, M.R., and Mainen, Z.F. (2017). Transient inhibition and long-term facilitation of locomotion by phasic optogenetic activation of serotonin neurons. ELife *6*, 1–26.

Cui, G., Jun, S.B., Jin, X., Pham, M.D., Vogel, S.S., Lovinger, D.M., and Costa, R.M. (2013). Concurrent activation of striatal direct and indirect pathways during action initiation. Nature *494*, 238–242.

Dayan, P., and Huys, Q. (2015). Serotonin's many meanings elude simple theories. ELife *4*, 3–5.

Deakin, J.F., and Graeff, F.G. (1991). 5-HT and mechanisms of defence. Journal of Psychopharmacology (Oxford, England) *5*, 305–315.

Doya, K. (2008). Modulators of decision making. Nature Neuroscience *11*, 410–416.

Eshel, N., Bukwich, M., Rao, V., Hemmelder, V., Tian, J., and Uchida, N. (2015). Arithmetic and local circuitry underlying dopamine prediction errors. Nature *525*, 243–246.

Fadok, J.P., Krabbe, S., Markovic, M., Courtin, J., Xu, C., Massi, L., Botta, P., Bylund, K., Müller, C., Kovacevic, A., et al. (2017). A competitive inhibitory circuit for selection of active and passive fear responses. Nature.

Fanselow, M.S., and Lester, L.S. (1988). A functional behavioristic approach to aversively motivated behavior: Predatory imminence as a determinant of the topography of defensive behavior. Evolution and Learning 185–212.

Flavell, S.W., Pokala, N., Macosko, E.Z., Albrecht, D.R., Larsch, J., and Bargmann, C.I. (2013). Serotonin and the Neuropeptide PDF Initiate and Extend Opposing Behavioral States in C. elegans. Cell *154*, 1023–1035.

Fonseca, M.S., Murakami, M., and Mainen, Z.F. (2015). Activation of Dorsal Raphe Serotonergic Neurons Promotes Waiting but Is Not Reinforcing. Current Biology *25*, 306–315.

De Franceschi, G., Vivattanasarn, T., Saleem, A.B., and Solomon, S.G. (2016). Vision Guides Selection of Freeze or Flight Defense Strategies in Mice. Current Biology : CB *26*, 2150–2154.

Fu, W., Le Maître, E., Fabre, V., Bernard, J.-F., David Xu, Z.-Q., and Hökfelt, T. (2010). Chemical neuroanatomy of the dorsal raphe nucleus and adjacent structures of the mouse brain. The Journal of Comparative Neurology *518*, 3464–3494.

Gentry, R.N., Lee, B., and Roesch, M.R. (2016). Phasic dopamine release in the rat nucleus accumbens predicts approach and avoidance performance. Nature Communications *7*, 13154.

Glickstein, M., and Stein, J. (1991). Paradoxical movement in Parkinson's disease. Trends in Neurosciences *14*, 480–482.

Grahn, R.E., Will, M.J., Hammack, S.E., Maswood, S., McQueen, M.B., Watkins, L.R., and Maier, S.F. (1999). Activation of serotonin-immunoreactive cells in the dorsal raphe nucleus in rats exposed to an uncontrollable stressor. Brain Research *826*, 35–43.

Greenwood, B.N., Foley, T.E., Le, T. V., Strong, P. V., Loughridge, A.B., Day, H.E.W., and Fleshner, M. (2011). Long-term voluntary wheel running is rewarding and produces plasticity in the mesolimbic reward pathway. Behavioural Brain Research *217*, 354–362.

Gunaydin, L.A., Grosenick, L., Finkelstein, J.C., Kauvar, I. V, Fenno, L.E., Adhikari, A., Lammel, S., Mirzabekov, J.J., Airan, R.D., Zalocusky, K.A., et al. (2014). Natural neural projection dynamics underlying social behavior. Cell *157*, 1535–1551.

Hayashi, K., Nakao, K., and Nakamura, K. (2015). Appetitive and Aversive Information Coding in the Primate Dorsal Raphe Nucleus. Journal of Neuroscience *35*, 6195–6208.

Hernández-Vázquez, F., Garduño, J., and Hernández-López, S. (2019). GABAergic modulation of serotonergic neurons in the dorsal raphe nucleus. Rev Neurosci *30*, 289–303.

Howard, C.E., Chen, C.-L., Tabachnik, T., Hormigo, R., Ramdya, P., and Mann, R.S. (2019). Serotonergic Modulation of Walking in Drosophila. Current Biology *29*, 4218-4230.e8.

Huang, L., Yuan, T., Tan, M., Xi, Y., Hu, Y., Tao, Q., Zhao, Z., Zheng, J., Han, Y., Xu, F., et al. (2017). A retinoraphe projection regulates serotonergic activity and looming-evoked defensive behaviour. Nature Communications *8*, 14908.

Jankowski, M.P., and Sesack, S.R. (2004). Prefrontal cortical projections to the rat dorsal raphe nucleus: ultrastructural features and associations with serotonin and gamma-aminobutyric acid neurons. The Journal of Comparative Neurology *468*, 518–529.

Jin, Z., Chen, X.-F., Ran, Y., Li, X.-R., Xiong, J., Zheng, Y., Gao, N., and Li, Y.-F. (2017). Mouse strain differences in SSRI sensitivity correlate with serotonin transporter binding and function. Scientific Reports *7*, 8631.

de Jong, J.W., Afjei, S.A., Pollak Dorocic, I., Peck, J.R., Liu, C., Kim, C.K., Tian, L., Deisseroth, K., and Lammel, S. (2019). A Neural Circuit Mechanism for Encoding Aversive Stimuli in the Mesolimbic Dopamine System. Neuron *101*, 133-151.e7.

Kawashima, T., Zwart, M.F., Yang, C.-T., Mensh, B.D., and Ahrens, M.B. (2016). The Serotonergic System Tracks the Outcomes of Actions to Mediate Short-Term Motor Learning. Cell *167*, 933-946.e20.

Keefe, K.A., Salamone, J.D., Zigmond, M.J., and Stricker, E.M. (1989). Paradoxical kinesia in parkinsonism is not caused by dopamine release: Studies in an animal model. Archives of Neurology *46*, 1070–1075.

Krabbe, S., Paradiso, E., d'Aquin, S., Bitterman, Y., Courtin, J., Xu, C., Yonehara, K., Markovic, M., Müller, C., Eichlisberger, T., et al. (2019). Adaptive disinhibitory gating by VIP interneurons permits associative learning. Nature Neuroscience *22*, 1834–1843.

Kramer, D.L., and McLaughlin, R.L. (2001). The Behavioral Ecology of Intermittent Locomotion. Integr Comp Biol *41*, 137–153.

Larsen, R.S., and Waters, J. (2018). Neuromodulatory Correlates of Pupil Dilation. Front. Neural Circuits *12*.

Lemos, J.C., Wanat, M.J., Smith, J.S., Reyes, B. a S., Hollon, N.G., Van Bockstaele, E.J., Chavkin, C., and Phillips, P.E.M. (2012). Severe stress switches CRF action in the nucleus accumbens from appetitive to aversive. Nature *490*, 402–406.

Letzkus, J.J., Wolff, S.B.E., Meyer, E.M.M., Tovote, P., Courtin, J., Herry, C., and Lüthi, A. (2011). A disinhibitory microcircuit for associative fear learning in the auditory cortex. Nature *480*, 331–335.

Lu, J., Li, C., Singh-Alvarado, J., Zhou, Z.C., Fröhlich, F., Mooney, R., and Wang, F. (2018). MIN1PIPE: A Miniscope 1-Photon-Based Calcium Imaging Signal Extraction Pipeline. Cell Reports *23*, 3673–3684.

Maier, S.F., and Watkins, L.R. (2005). Stressor controllability and learned helplessness: the roles of the dorsal raphe nucleus, serotonin, and corticotropin-releasing factor. Neuroscience and Biobehavioral Reviews *29*, 829–841.

Marshall, J.F., Levitan, D., and Stricker, E.M. (1976). Activation-induced restoration of sensorimotor functions in rats with dopamine-depleting brain lesions. Journal of Comparative and Physiological Psychology *90*, 536–546.

Maswood, S., Barter, J.E., Watkins, L.R., and Maier, S.F. (1998). Exposure to inescapable but not escapable shock increases extracellular levels of 5-HT in the dorsal raphe nucleus of the rat. Brain Research *783*, 115–120.

Mathis, M.W., and Mathis, A. (2019). Deep learning tools for the measurement of animal behavior in neuroscience. ArXiv:1909.13868 [Cs, q-Bio].

Miller, T., Clements, K., Ahn, S., Park, C., Hye Ji, E., and Issa, F.A. (2017). Social status-dependent shift in neural circuit activation affects decision-making. The Journal of Neuroscience *37*, 1548–16.

Miyazaki, K., Miyazaki, K.W., and Doya, K. (2011). Activation of dorsal raphe serotonin neurons underlies waiting for delayed rewards. J. Neurosci. *31*, 469–479.

Miyazaki, K.W., Miyazaki, K., and Doya, K. (2012). Activation of dorsal raphe serotonin neurons is necessary for waiting for delayed rewards. J. Neurosci. *32*, 10451–10457.

Miyazaki, K.W., Miyazaki, K., Tanaka, K.F., Yamanaka, A., Takahashi, A., Tabuchi, S., and Doya, K. (2014). Optogenetic activation of dorsal raphe serotonin neurons enhances patience for future rewards. Curr. Biol. *24*, 2033–2040.

Niv, Y., Daw, N.D., Joel, D., and Dayan, P. (2007). Tonic dopamine: opportunity costs and the control of response vigor. Psychopharmacology *191*, 507–520.

Ogawa, S.K., Cohen, J.Y., Hwang, D., Uchida, N., and Watabe-Uchida, M. (2014). Organization of monosynaptic inputs to the serotonin and dopamine neuromodulatory systems. Cell Rep *8*, 1105–18.

Oleson, E.B., Gentry, R.N., Chioma, V.C., and Cheer, J.F. (2012). Subsecond Dopamine Release in the Nucleus Accumbens Predicts Conditioned Punishment and Its Successful Avoidance. J. Neurosci. *32*, 14804–14808.

Pediatric OCD Treatment Study (POTS) Team (2004). Cognitive-behavior therapy, sertraline, and their combination for children and adolescents with obsessive-compulsive disorder: the Pediatric OCD Treatment Study (POTS) randomized controlled trial. JAMA *292*, 1969–1976.

Politis, D.N., and Romano, J.P. (1994). The Stationary Bootstrap. Journal of the American Statistical Association *89*, 1303–1313.

Pultorak, K.J., Schelp, S.A., Isaacs, D.P., Krzystyniak, G., and Oleson, E.B. (2018). A Transient Dopamine Signal Represents Avoidance Value and Causally Influences the Demand to Avoid. ENeuro *5*.

Ren, J., Friedmann, D., Xiong, J., Liu, C.D., Ferguson, B.R., Weerakkody, T., DeLoach, K.E., Ran, C., Pun, A., Sun, Y., et al. (2018). Anatomically Defined and Functionally Distinct Dorsal Raphe Serotonin Sub-systems. Cell *175*, 472-487.e20.

Ren, J., Isakova, A., Friedmann, D., Zeng, J., Grutzner, S.M., Pun, A., Zhao, G.Q., Kolluru, S.S., Wang, R., Lin, R., et al. (2019). Single-cell transcriptomes and whole-brain projections of serotonin neurons in the mouse dorsal and median raphe nuclei. ELife *8*, e49424.

Salamone, J.D., and Correa, M. (2012). The mysterious motivational functions of mesolimbic dopamine. Neuron *76*, 470–485.

Sherwin, C.M. (1998). Voluntary wheel running: a review and novel interpretation. Animal Behaviour *56*, 11–27.

Souques, M.A. (1921). Rapport sur les syndrome parkinsoniens. Rev Neurol *28*, 534–573.

Strekalova, T., Spanagel, R., Bartsch, D., Henn, F.A., and Gass, P. (2004). Stress-induced anhedonia in mice is associated with deficits in forced swimming and exploration. Neuropsychopharmacology *29*, 2007–2017.

Takahashi, A., Shimamoto, A., Boyson, C.O., DeBold, J.F., and Miczek, K. a. (2010). GABAB Receptor Modulation of Serotonin Neurons in the Dorsal Raphe Nucleus and Escalation of Aggression in Mice. J. Neurosci. *30*, 11771–11780.

Vong, L., Ye, C., Yang, Z., Choi, B., Chua, S., and Lowell, B.B. (2011). Leptin action on GABAergic neurons prevents obesity and reduces inhibitory tone to POMC neurons. Neuron *71*, 142–154.

Warden, M.R., Selimbeyoglu, A., Mirzabekov, J.J., Lo, M., Thompson, K.R., Kim, S.-Y., Adhikari, A., Tye, K.M., Frank, L.M., and Deisseroth, K. (2012). A prefrontal cortex–brainstem neuronal projection that controls response to behavioural challenge. Nature *492*, 428–432.

Wiltschko, A.B., Johnson, M.J., Iurilli, G., Peterson, R.E., Katon, J.M., Pashkovski, S.L., Abraira, V.E., Adams, R.P., and Datta, S.R. (2015). Mapping Sub-Second Structure in Mouse Behavior. Neuron *88*, 1121–1135.

Zhou, L., Liu, M.-Z., Li, Q., Deng, J., Mu, D., and Sun, Y.-G. (2017). Organization of Functional Long-Range Circuits Controlling the Activity of Serotonergic Neurons in the Dorsal Raphe Nucleus. Cell Reports *18*, 3018–3032.

Zhuang, X., Masson, J., Gingrich, J.A., Rayport, S., and Hen, R. (2005). Targeted gene expression in dopamine and serotonin neurons of the mouse brain. J. Neurosci. *143*, 27–32.